ADVANCED MATERIALS
www.advmat.de

Monolithic Perovskite-Silicon Tandem Solar Cells: From the Lab to Fab?

Fan Fu, Jia Li, Terry Chien-Jen Yang, Haoming Liang, Antonin Faes, Quentin Jeangros, Christophe Ballif, and Yi Hou**

This review focuses on monolithic 2-terminal perovskite-silicon tandem solar cells and discusses key scientific and technological challenges to address in view of an industrial implementation of this technology. The authors start by examining the different crystalline silicon (c-Si) technologies suitable for pairing with perovskites, followed by reviewing recent developments in the field of monolithic 2-terminal perovskite-silicon tandems. Factors limiting the power conversion efficiency of these tandem devices are then evaluated, before discussing pathways to achieve an efficiency of >32%, a value that small-scale devices will likely need to achieve to make tandems competitive. Aspects related to the upscaling of these device active areas to industry-relevant ones are reviewed, followed by a short discussion on module integration aspects. The review then focuses on stability issues, likely the most challenging task that will eventually determine the economic viability of this technology. The final part of this review discusses alternative monolithic perovskite-silicon tandem designs. Finally, key areas of research that should be addressed to bring this technology from the lab to the fab are highlighted.

1. Introduction

Photovoltaics (PV), which directly converts solar energy into electricity, offers a clean and sustainable solution to meet ever-increasing global energy demands. Today, solar electricity accounts for only ≈3% of global electricity generation.[1] However, PV is experiencing an accelerated growth globally with >130 GW installed in 2020, an acceleration that should continue in the future to provide 20–30% of the global electricity on the 2050 horizon.[2] The key to materializing this ambitious goal is to reduce the cost of PV-generated electricity to make solar energy significantly cheaper than that produced by fossil fuels, and to promote the implementation of storage technologies.[3] Currently, the major cost component of a PV system stems from the balance-of-systems (BOS).[4] The BOS refers to all the components of a PV system other than the solar module, including wiring, inverters, land, installation, labor, etc. With cell costs typically accounting for less than 20% of the total module cost (and module costs typically account for around 40% at the system level),[4,5] increasing power conversion efficiency at the cell and module level is the most efficient way to reduce the levelized cost of electricity (LCOE), provided this efficiency gain comes at affordable manufacturing costs.[6] Increasing the solar module efficiency is even more important for residential rooftops, facades, or other applications where

F. Fu, T. C.-J. Yang,[+] Q. Jeangros, C. Ballif
École Polytechnique Fédérale de Lausanne (EPFL)
Institute of Microengineering (IMT)
Photovoltaics and Thin-Film Electronics Laboratory (PV-Lab)
Rue de la Maladière 71b, Neuchâtel 2002, Switzerland
E-mail: fan.fu@empa.ch

F. Fu
Laboratory for Thin Films and Photovoltaics
Empa—Swiss Federal Laboratories for Materials Science and Technology
Überlandstrasse 129, Dübendorf 8600, Switzerland

The ORCID identification number(s) for the author(s) of this article can be found under https://doi.org/10.1002/adma.202106540.

[+]Present address: Department of Chemical Engineering & Biotechnology, University of Cambridge, Philippa Fawcett Drive, Cambridge CB3 0AS, UK

DOI: 10.1002/adma.202106540

J. Li, H. Liang, Y. Hou
Solar Energy Research Institute of Singapore (SERIS)
National University of Singapore
7 Engineering Drive 1, Singapore 117574, Singapore
E-mail: yi.hou@nus.edu.sg

T. C.-J. Yang
CSIRO Energy Centre
10 Murray Dwyer Circuit, Mayfield West
New South Wales 2304, Australia

H. Liang, Y. Hou
Department of Chemical and Biomolecular Engineering
National University of Singapore
4 Engineering Drive 4, Singapore 117585, Singapore

A. Faes, Q. Jeangros, C. Ballif
PV-Center
CSEM
Jaquet-Droz 1, Neuchâtel 2002, Switzerland

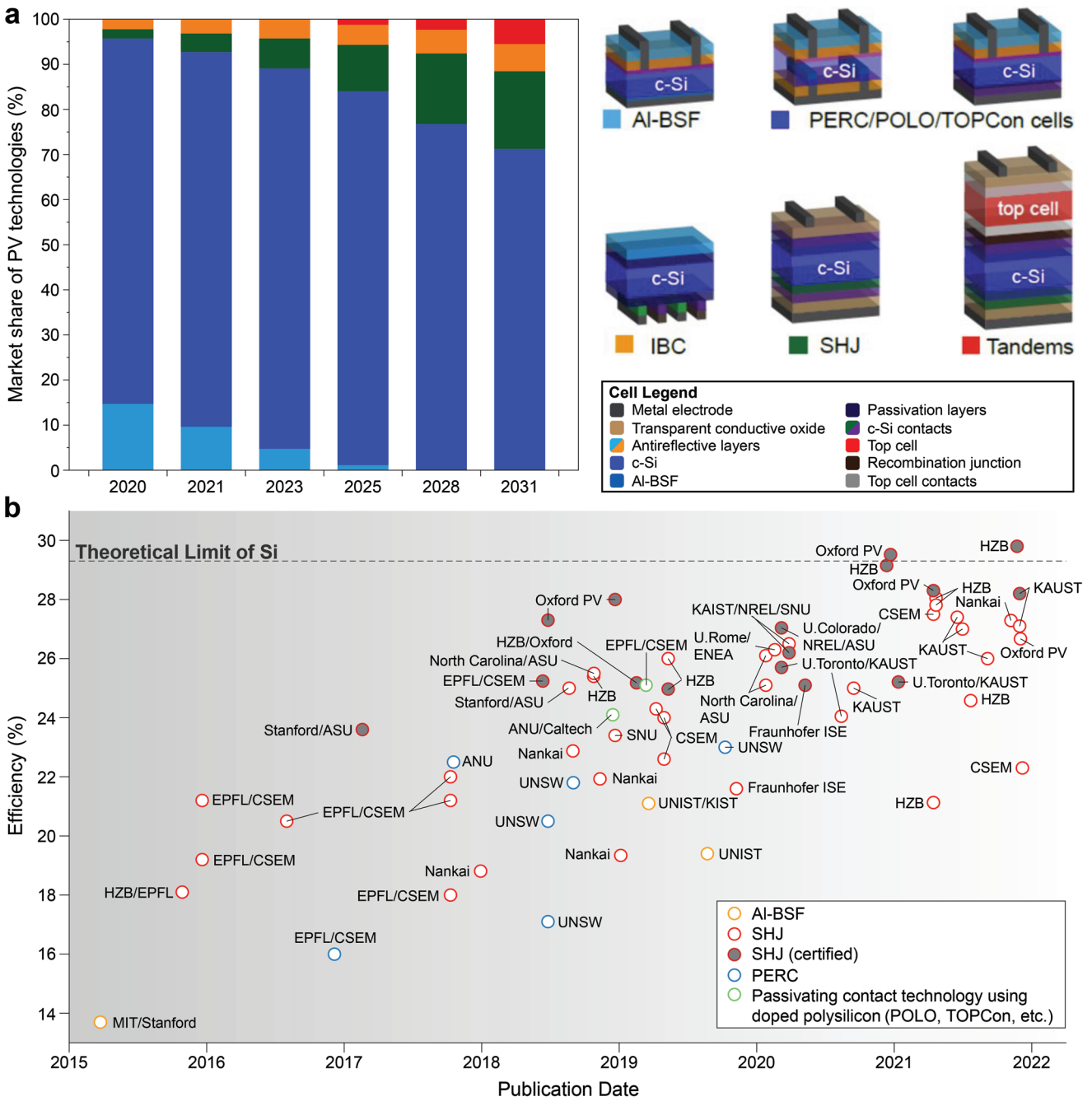

Figure 1. Monolithic perovskite-silicon tandem solar cells. a) ITRPV market share predictions of the different c-Si-based PV technologies (April 2021) alongside schematic drawings of the different cell architectures.[4] b) Efficiency evolution of monolithic perovskite-silicon tandem solar cells. Yellow: Al back surface field (Al-BSF); blue: passivated emitter and rear contact (PERC); green: passivating contact technology using doped polysilicon; red: silicon heterojunction (SHJ); open symbols: in-house measurements; solid symbols: independently certified values.

space is limited or where the balance of systems costs per watt are higher,[7] opening up promising markets for novel high-end PV technologies.

Crystalline silicon (c-Si) PV technologies have been dominating the PV market for decades now (current market share of ≈95%) owing to their high module efficiencies, abundance, and non-toxicity of the constituent elements, as well as, long-term reliability.[8,9] In recent years, the power conversion efficiency of industrial c-Si solar cells has continued to increase thanks to the advent of device designs based on the passivated emitter and rear cells (PERC).[10–12] PERC makes now for the major part of the c-Si market, substituting to cells based on the aluminum back-surface field (Al-BSF) technology, as illustrated in **Figure 1**a. The cell efficiency can be increased further by using high-temperature passivating contacts[13–16] (e.g., tunnel oxide passivated contact, TOPCon, or polysilicon on oxide, POLO) or a

silicon heterojunction cell (SHJ) design.[17] Additional efficiency gains have been achieved by placing all the contacts at the rear of these cells in an interdigitated back contacted (IBC) design to avoid shadow losses.[18] In March 2017, Kaneka Corporation reported a certified record efficiency of 26.7% for a single-junction SHJ solar cell in the IBC configuration.[19] However, efficiency gains by optimizing the c-Si cell design will not continue for much longer, at least at the R&D level, as the practical efficiency limit of the technology stands just above 27% taken into account extrinsic recombination loss, optical loss, and resistive loss.[19] c-Si solar cells are limited by Auger recombination to a theoretical efficiency limit of 29.56%,[20,21] which sets a clear stop for the efficiency learning curve of c-Si PV.

Designing cells that achieve an efficiency beyond 30% will require a change to the line of action. The most promising approach to overcome this efficiency barrier under one sun conditions involves stacking a wider bandgap absorber on top of c-Si to make a tandem solar cell (Figure 1a). The wide bandgap top cell will absorb the high-energy photons with reduced thermalization losses, with the narrow bandgap c-Si bottom cell absorbing the low-energy photons of the solar spectrum.[22] The tandem solar cells can be constructed in either 2-terminal configuration, where wide-bandgap subcell is monolithically grown on top of narrow bandgap Si subcell, and 4-terminal configuration, where the two subcells are fabricated independently and mechanically stacked together. Although 4-terminal tandems are easy to prototype, they suffer from severe parasitic optical losses due to the use of 3 layers of transparent conducting oxide (TCO) and higher costs due to the use of two independent circuits. While 2-terminal tandems consist of two series-connected subcells, therefore one circuit and fewer TCO layers are needed, and the open-circuit voltage (V_{OC}) of the tandems will be the sum of V_{OC} of each subcell and the short circuit current of the tandems will be limited by the lowest value of the subcell (so-called "current matching"). More detailed comparisons of 4-terminal and 2-terminal tandems could be found elsewhere.[23] The theoretical efficiency limit for a Si-based tandem cell is ≈45%, a value much higher than the c-Si single-junction limit detailed above.[24] At the experimental level, stacking a GaAs top cell on c-Si to form a 4-terminal tandem has resulted in efficiencies of 32.8%, whereas triple junctions featuring two III–V cells on Si reached 35.9% and 33.3% in a 4-terminal and 2-terminal configuration, respectively.[25,26] However, the scarcity and the high cost of the III-V top cell materials make such cell designs unlikely to target large volumes.[27,28] Still, these values provide an estimate of the efficiencies that alternative multi-junction designs featuring cheaper constituents should achieve.

With a broadly tunable bandgap[29] and high initial efficiency at the single-junction level (currently 25.5% for a cell area of 0.095 cm^2),[30] metal halide perovskites are ideal alternatives to III–V materials for a tandem integration with c-Si. Adopting perovskite crystal structure with a general chemical formula of ABX_3, metal halide perovskites typically contain widely available cations and anions: methylammonium (CH_3NH_3, MA), formamidinium ($CH(NH_2)_2$, FA), and/or cesium (Cs) on the A site, Pb and/or Sn on the B site, and Cl, Br, and/or I on the X site.[23] Thanks to advantageous defect tolerance,[31,32] high-quality perovskite absorbers can be grown at low temperatures (usually <150 °C), enabling their deposition on high-efficiency c-Si cells to form monolithic 2-terminal tandems. This means that c-Si process lines could be refurbished to include the extra process steps to deposit the perovskite top cells, naturally extending the c-Si learning curve. It is worth noting that process incompatibilities complicate a similar extension of c-Si with a III–V top cell: III–V-on-c-Si tandems are often limited to 4-terminal designs[25] or require wafer bonding[26] as sub-cells must be processed independently to achieve high performance. Though 4-terminal designs have certain advantages (independent sub-cell processing widening the choice of materials and processes, absence of sub-cell current mismatch losses), they also involve additional system costs (wires, inverters) and require two extra transparent electrodes that may compromise optical performance. Based on these considerations, monolithic 2-terminal tandems are regarded as more promising from an industrial perspective and will hence be the focus of this review.

Since they were first reported in 2015, 2-terminal monolithic perovskite-silicon tandem solar cells have quickly progressed, as shown in Figure 1b and Table S1, Supporting Information.[33–41] For more details about the material chemistry of perovskite in tandems, we refer the reader to the extensive review by Eperon et al.[36] and Anaya et al.[34] For the detailed guidelines for future developments and commercialization of tandem, we refer the reader to the review by Werner et al.[35] Regarding the potential of perovskite tandem solar cells, we refer the reader to the review by Leijtens et al.[33] Hossain et al.[39] derived guideline for the optimization of perovskite solar cells and discussed the influence of photon management. Later in 2020, Shen et al.[37] suggest the path toward >30% efficiency by combining optical modeling and electrical modeling on the cells. Jost et al.[38] summarized the advanced structural, electrical, optical, radiative, and electronic characterization methods and simulations on tandems. Very recently, Chen et al. reviewed the efficiency evaluation of perovskite/silicon tandems, point out the solutions for improving the efficiency and reducing the costs. Notably, in June 2018, Oxford PV announced a certified efficiency of 27.3% (≈1 cm^2) for a perovskite-silicon tandem device, surpassing for the first time the c-Si efficiency record.[42] Certified efficiencies are now as high as 29.2% (HZB)[43] and 29.5% (Oxford PV).[44] During the revision of the manuscript, the efficiency of perovskite-silicon monolithic tandem was further raised to 29.8% (HZB).[44] The milestone of 30% is now well in sight and perovskite-silicon tandems are starting to fulfill their efficiency potential.

Despite their promises, there are still many pressing challenges to overcome before perovskite-silicon tandems can become commercial products. To ease the perovskite integration into c-Si process lines, the perovskite top cell most likely be made as compatible as possible with existing c-Si bottom cell technologies. Ideally, the perovskite should be deposited directly on the micron-sized pyramidal texture of c-Si cells, a texture that reduces reflection losses and promotes light-trapping. However, depositing a high-quality perovskite absorber on standard c-Si pyramids has proven challenging as these features are typically one order of magnitude larger than the perovskite thickness. In fact, most of the reported monolithic perovskite-silicon tandems circumvent this issue by employing wafers that are mechanically or chemically polished on their front side to enable standard solution processing of the perovskite.[45,46]

While enabling high performance, this design concession leads to optical losses unless additional elements are introduced in the cell (e.g., an antireflective foil). Another issue is that the aforementioned record devices and the vast majority of the perovskite-silicon tandems reported to date have lab-scale dimensions (≈1 cm^2), and most devices are produced by spin coating the perovskite absorber, a method that is unlikely to yield layers of the required quality on 6-inch c-Si wafers with the required throughput. Therefore, industrial manufacturing methods that can yield high-efficiency top cells on 6-inch c-Si wafers must be developed. In addition, module assembly techniques will also need to be adapted to ensure that not only cells but also modules achieve efficiency targets. And maybe most importantly, as long-term stability will finally dictate the economic viability of perovskite-silicon tandem cells,[47] perovskite-silicon tandems will likely need to reach operational stability comparable to that of c-Si single-junction cells (>25 years). This review discusses these challenges as well as the most promising strategies to produce perovskite-silicon monolithic tandem solar cells and modules with combined high efficiency and long-term stability.

2. Monolithic Perovskite-Silicon Tandems: Complementary and Compatible Building Blocks

This part discusses how the different building blocks of 2-terminal perovskite-silicon tandems, namely the c-Si bottom cell, the recombination junction, and the perovskite top cell, have been combined to achieve maximum performance and compatibility with existing c-Si process flows.

2.1. Silicon Cells for Tandems

According to the ITRPV's market share predictions (Figure 1a),[4] a certain number of c-Si cell technologies could suitably partner perovskites in c-Si-based tandems. The now outdated Al-BSF technology is an unlikely candidate given that it is currently being phased out and replaced by PERCs. The latter c-Si technology is estimated to rise to a market share of >70% in 2030 (N.B. the ITRPV has included TOPCon, POLO, or high temperature passivating contacted cells within the PERC family). Another excellent candidate is the SHJ technology, which is estimated to take a market share of about 15% in 2030. All three technologies (PERC, TOPCon, and SHJ) are suitable candidates for monolithic perovskite-silicon tandem solar cells,[48] as discussed below. Furthermore, IBCs, which are predicted to take a market share of ≈5% in 2030, could also be used in a 3-terminal design, as discussed at the end of this review.

PERC's main advantages for tandems are their market dominance and higher temperature tolerance, making them compatible with perovskite deposition processes requiring high temperatures, for example, to sinter a TiO_2 or SnO_2 electron transport layer (ETL).[49,50] However, some adaptations to the PERC design are needed to accommodate a perovskite top cell. Indeed, PERCs consist of a dielectric layer on their front surface (typically SiN_x, sometimes combined with AlO_x). While providing excellent surface passivation as well as antireflection properties, its insulating nature complicates the sub-cell interconnection in a monolithic tandem configuration. One option is to replace this dielectric layer stack with a transparent conductive oxide (TCO) but this has been shown to lead to substantial losses in open-circuit voltage (V_{OC}) in tandems.[51,52] To mitigate surface recombination and improve V_{OC}, one possibility is to create local openings in the SiN_x(/AlO_x) stack, for example, using photolithography, followed by the deposition of a conductive pathway, an approach that enabled the demonstration of 22.5%-efficient tandems.[50] A simpler approach involves contacting the p+ emitter of an n-type cell directly with the TiO_x ETL of the perovskite top cell, yielding tandems reaching an efficiency of 24.1%.[53] For n+ emitters, an alternative relies on the replacement of the standard diffused junction and the dielectric SiN_x with a high temperature passivating SiO_x/n^+ polysilicon contact.[54] The stack can be capped with a p^+ poly-Si layer to form a tunnel junction to connect the two sub-cells. High-temperature passivating contacts may also be used on both sides of the c-Si wafer, yielding 25.1%-efficient monolithic tandems when employing a p-type c-Si wafer.[55]

SHJs are gaining increasing attention due to their high efficiency and simpler fabrication process.[56,57] As illustrated in **Figure 2**a, SHJ solar cells consist of a c-Si wafer (typically n-type) that is passivated by intrinsic and doped hydrogenated amorphous silicon (a-Si:H) layers. The doped a-Si:H layers are then capped by a TCO on both sides, before finishing the device with an Ag metal grid on the front side and an Ag reflector on the rear side. Compared to PERCs and cell designs based on high-temperature passivating contacts, SHJs exhibit a higher open-circuit voltage (up to 750 mV),[58] excellent near-infrared response,[59] a lower temperature coefficient,[56] but also lower photocurrent due to parasitic absorption of blue light in the front a-Si:H/TCO stack.[60] In a tandem device, the latter losses can be mitigated as blue light is absorbed in the front perovskite sub-cell. Additionally, the top TCO layer can be adapted to form the recombination junction as discussed below. Finally, SHJs can be produced in various configurations, with either the electron or the hole selective contact being deposited at the front of the cell. Overall, these advantages and this flexibility have made SHJs the most widely employed bottom cell technology in tandems with perovskites. All reported tandems exhibiting an efficiency >25% employ an (n-type) SHJ bottom cell,[61–70] with the notable exception of ref. [55], which details a tandem based on a p-type wafer sandwiched with high-temperature passivating contacts. Still, one drawback of SHJs is their inability to withstand processing temperatures >250 °C. Hydrogen effuses out of a-Si:H layers in these conditions and passivation is lost, hence requiring the development of low-temperature perovskite deposition processes.

2.2. Sub-cell Interconnection

As in monolithic tandem devices, both top cells and bottom cells have the same architecture, for example, both p-i-n structure, if the two cells are simply stacked, a p-i-n-p-i-n structure will form, a counter n-p junction in between will form an energy barrier to carrier transporting.[71,72] Thus a barrier-free connection between the top and bottom sub-cells, in this case

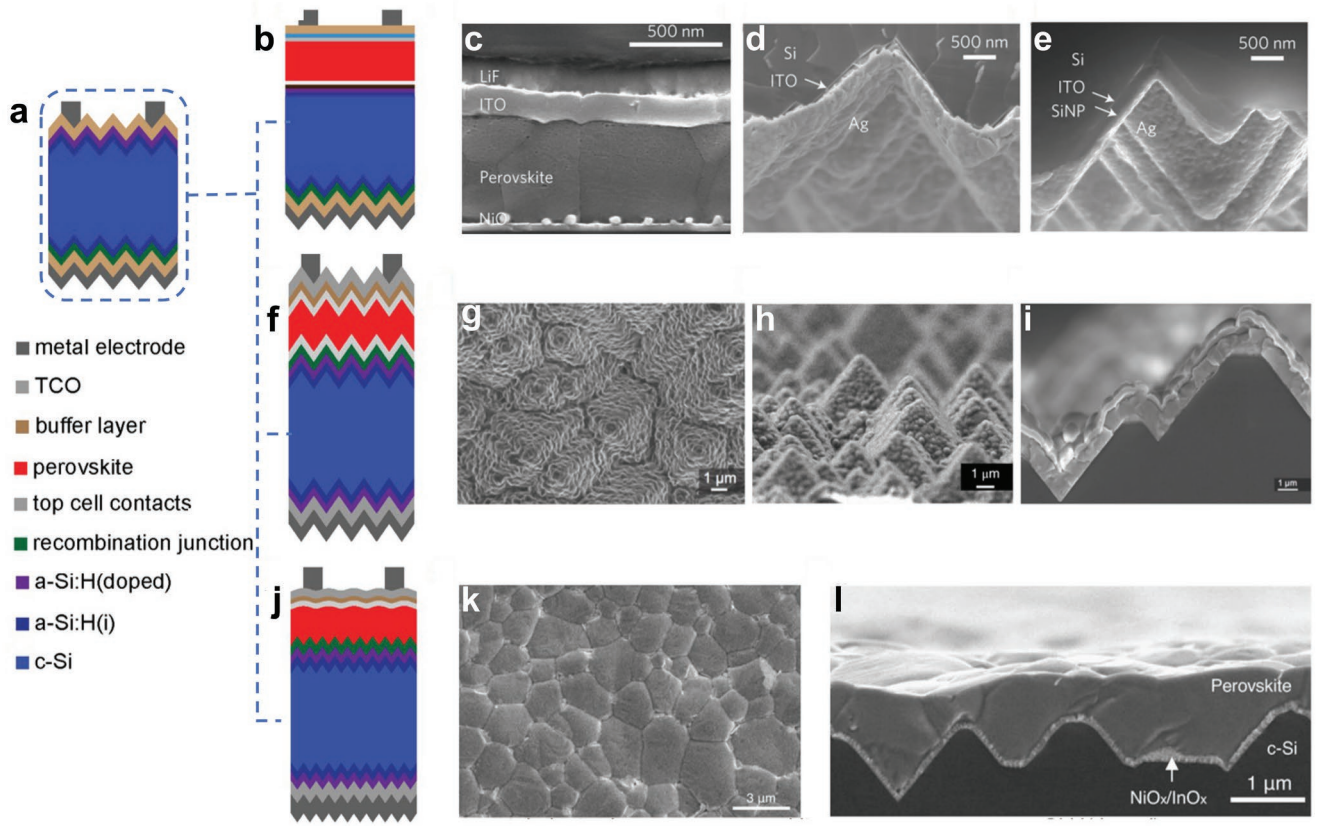

Figure 2. Monolithic perovskite-SHJ tandems. a) Schematic illustration of a SHJ cell in rear emitter configuration. b) Device structure and cross-section scanning electron microscopy (SEM) images of a tandem cell featuring a front side-polished c) and rear side-textured c-Si wafer d) with and e) without silicon nanoparticles. f) The device structure of a fully textured monolithic perovskite-SHJ tandem cell. SEM images of the perovskite cell deposited on textured c-Si, g) top-view, h) tilted-view, and i) cross-section. j) The device structure of a solution-processed perovskite on a textured c-Si wafer. SEM k) top-view and l) cross-section images of solution-processed perovskite covering the texture of c-Si (average pyramid size of 2 µm). a,b,e,i–k) Reproduced with permission.[66] Copyright 2020, The American Association for the Advancement of Science. c,d) Reproduced with permission.[80] Copyright 2017, Springer Nature. f–h) Reproduced with permission.[75] Copyright 2018, Springer Nature.

between the perovskite and c-Si, is required. Two main types of barrier-free interconnection layers have been employed, namely (1) tunnel junctions and (2) recombination layers. Tunnel junctions have been developed for III-V and silicon multi-junction solar cells.[73,74] They are composed of a pair of highly doped p^+ and n^+ semiconducting layers, for example, a nanocrystalline hydrogenated silicon tunnel junction (nc-Si:H(n^+)/ nc-Si:H(p^+)) was adopted by Sahli et al.,[75] which form a very narrow depletion region at the contact area and thus enable interband tunneling (and recombination) of charge carriers at their interface. On the other hand, recombination layers are typically composed of an electron-conducting TCO[43,66,68] that makes an ohmic contact with the adjacent hole and electron-selective layers, with photogenerated carriers recombining at the TCO/hole-selective layer interface.

2.3. Adapting the Perovskite Top Cell to the c-Si Cell

The first monolithic perovskite-silicon tandem cell was reported by Mailoa et al.[76] in March 2015. It consisted of a high temperature-processed (~500 °C) mesoscopic perovskite top cell and a front side-polished Si homojunction bottom cell connected by a Si-based tunnel junction. A stabilized efficiency of 13.7% was achieved with a 1 cm^2 tandem cell. The V_{OC} reached 1.65 V, while the J_{SC} was limited to 11.5 mA/cm^2. Later, in October 2015, Albrecht et al.[77] developed a low temperature-processed (< 200 °C) planar perovskite top cell, enabling the use of a SHJ bottom cell to exploit its high V_{OC} and excellent infrared response. Using ITO as a recombination layer, an 18%-efficient monolithic tandem cell with a V_{OC} of 1.78 V and J_{SC} of 14 mA cm^{-2} was produced. Soon after, Werner et al.[78] employed a similar planar perovskite-SHJ tandem device structure and further raised the tandem efficiency to 21.2%. The efficiency gain resulted from an improved J_{SC} of 15.9 mA cm^{-2} thanks to the use of an anti-reflection foil on the front of the device and a pyramidal texture on the rear side of the wafer. All these monolithic tandems featured an n-i-p perovskite top cell, where incident light first passed through the hole transport layer (HTL) before reaching the perovskite absorber. One issue was the parasitic absorption of the high-energy photons in the thick Spiro-OMeTAD HTL, which strongly limited the J_{SC} and hence device performance.[79]

Due to a lack of transparent HTL alternatives that could be deposited on top of the perovskite, these optical losses stimulated the development of semi-transparent perovskite solar cells

deposited in the p-i-n configuration as these could feature a thinner ETL at the front to reduce parasitic absorption.[81,82] In 2017, Bush et al.[80] produced p-i-n cells by employing an atomic layer deposited (ALD) stack of SnO_2/zinc tin oxide on top of the ETL C60 to protect the perovskite from TCO sputtering damage. Combined with a SHJ bottom cell, they demonstrated a 23.6%-efficient monolithic perovskite-SHJ tandem cell with an active area of 1 cm^2 (NREL certified).[80] Importantly, the J_{SC} of the tandem cell was significantly improved to 18.7 mA cm^{-2} (without the use of an anti-reflection foil) thanks to the lower parasitic absorption in the top contact compared to n-i-p devices. This milestone triggered the widespread development of p-i-n perovskite top cells.[55,61,63–68,75,83–85]

The first set of tandem devices featured a front side-polished c-Si wafer to enable solution processing of the perovskite top cell and a textured rear side for enhanced light trapping of low-energy photons, as shown in Figure 2b–e. However, the absence of texture on the front side led to reflection losses and also affected light trapping (in addition to requiring an adaptation of the c-Si cell design). Sahli et al.[75] were the first to successfully report a functional perovskite top cell on a SHJ cell textured on both sides. This feat was achieved by replacing the conventional solution-based perovskite deposition with a hybrid thermal evaporation/spin-coating process (Figure 2f–i). A template layer was first conformally deposited on the ≈5 µm-high pyramidal features by co-evaporating PbI_2 and CsBr, followed by spin-coating a solution of FAI and FABr and subsequent annealing to form the perovskite layer. Using a nanocrystalline silicon tunnel junction, they demonstrated the first fully textured monolithic perovskite-SHJ tandem cell with a certified efficiency of 25.2% (1.42 cm^2 (designated area), certified by Fraunhofer ISE) and a high J_{SC} of 19.5 mA cm^{-2}. The reflection loss in the double-side textured tandem design was 1.64 mA cm^{-2}, the lowest value reported to date. Ross et al.[86] first used the co-evaporation method to fabricate perovskite/textured silicon tandem solar cells, where all the layers were made with scalable vacuum processes except a SAM layer as HTL.

Recently, alternative approaches to deposit perovskite absorbers on top of c-Si pyramids via solution processing have been demonstrated independently by Chen et al.[65] and Hou et al.[66] The main idea is to reduce the size of the c-Si texture and use micrometer-thick perovskite layers, deposited either by blade coating or spin coating, to completely cover the pyramids, as illustrated in Figure 2j–l. While optically not as performant as conformally coated textured designs, this approach still lowers reflection losses at the perovskite/c-Si interface compared to flat designs and improves the trapping of infrared light. The perovskite thickness at c-Si pyramid valleys is usually over a micrometer, hence requiring a high-quality absorber to ensure a sufficient charge carrier diffusion length to avoid collection losses. Hou et al.[66] introduced a self-limiting passivation agent on the perovskite top surface to improve material quality and unveiled a broadening of the depletion width at the pyramid base. Their cells achieved a certified efficiency of 25.7%. Similarly, Chen et al.[65] produced a tandem cell with a lab efficiency of 26% by blade-coating a perovskite layer on a textured SHJ. Also, Aydin et al.[87] fabricated 25% perovskite/textured silicon tandem solar cells by the spin-coating method, and they suggest that the optimal perovskite bandgap energy at standard test conditions is <1.68 eV for field performance at operational temperatures greater than 55 °C due to the opposite trend of the temperature dependence of both the silicon and perovskite bandgaps. Isikgor et al.[88] reported 27.4% perovskite/textured silicon tandem solar cells by the spin-coating method and a concurrent cationic and anionic perovskite defect passivation strategy.

Overall, these breakthroughs demonstrate that c-Si cells, especially SHJs, do not require any major modification to their design, not even to their front side texture, to accommodate a high-efficiency perovskite top cell. This direct compatibility between the technologies is an important aspect in view of the possible industrialization of tandems. However, it is worth noting that cell designs that feature a polished front side, despite being prone to additional optical losses, currently achieve higher performance at this stage thanks to higher V_{OC} and FF.[44,67] These optical losses in flat (or flattened) designs can be mitigated to some extend using a recombination junction stack with a finely tuned refractive index to manage infrared light[64] and a light management foil on the front side of the tandem.[62,63,89] However, these mitigation strategies come at the expense of device simplicity and direct compatibility with c-Si: industrial monocrystalline c-Si cells all feature a texture on their front side. Furthermore, these mitigation strategies do not bring the photocurrent of flat devices to the level of conformally coated textured ones. The next steps to fully materialize the efficiency potential of monolithic 2-terminal perovskite-silicon tandems will likely involve combining the high FF and V_{OC} of flat devices with the high J_{SC} of textured ones, as discussed below.

3. Toward >32%-Efficient Monolithic Tandems?

Perovskite-Si tandems are likely to lower LCOE compared to single-junction solar cells efficiently due to the higher efficiency potential. From the calculation by Messmer et al., >30%-efficient perovskite-Si tandems promise 11% lower of LCOE compared to the conventional PERC single-junction Si solar cells.[48] Meanwhile, the state-of-art GaAs-Si tandems have reached a certified efficiency of 32.8%,[90] which sets a practical target for perovskite-Si to catch up with. In this section, we review the literature and discuss some avenues that may achieve >32%-efficient monolithic perovskite-c-Si tandem solar cells.

3.1. Optical Design

Figure 3a compares the external quantum efficiency (EQE) spectra of several representative certified monolithic perovskite-SHJ tandems: the front side polished tandem of Xu et al. (reaching 25.8% with an anti-reflection foil),[67] the front side polished tandem of Al-Ashouri et al. (reaching 29.15% with an LiF anti-reflection coating),[44] the textured bottom cell coated by a solution-processed perovskite layer of Hou et al. (reaching 25.7% without any antireflective foil),[67] the conformally coated textured cell reported by Sahli et al. (25.2%),[75] and 29.5% cells of Oxford PV,[91] and a two-sides contacted SHJ solar cell from Kaneka for reference (25.1%).[17] The cumulative current

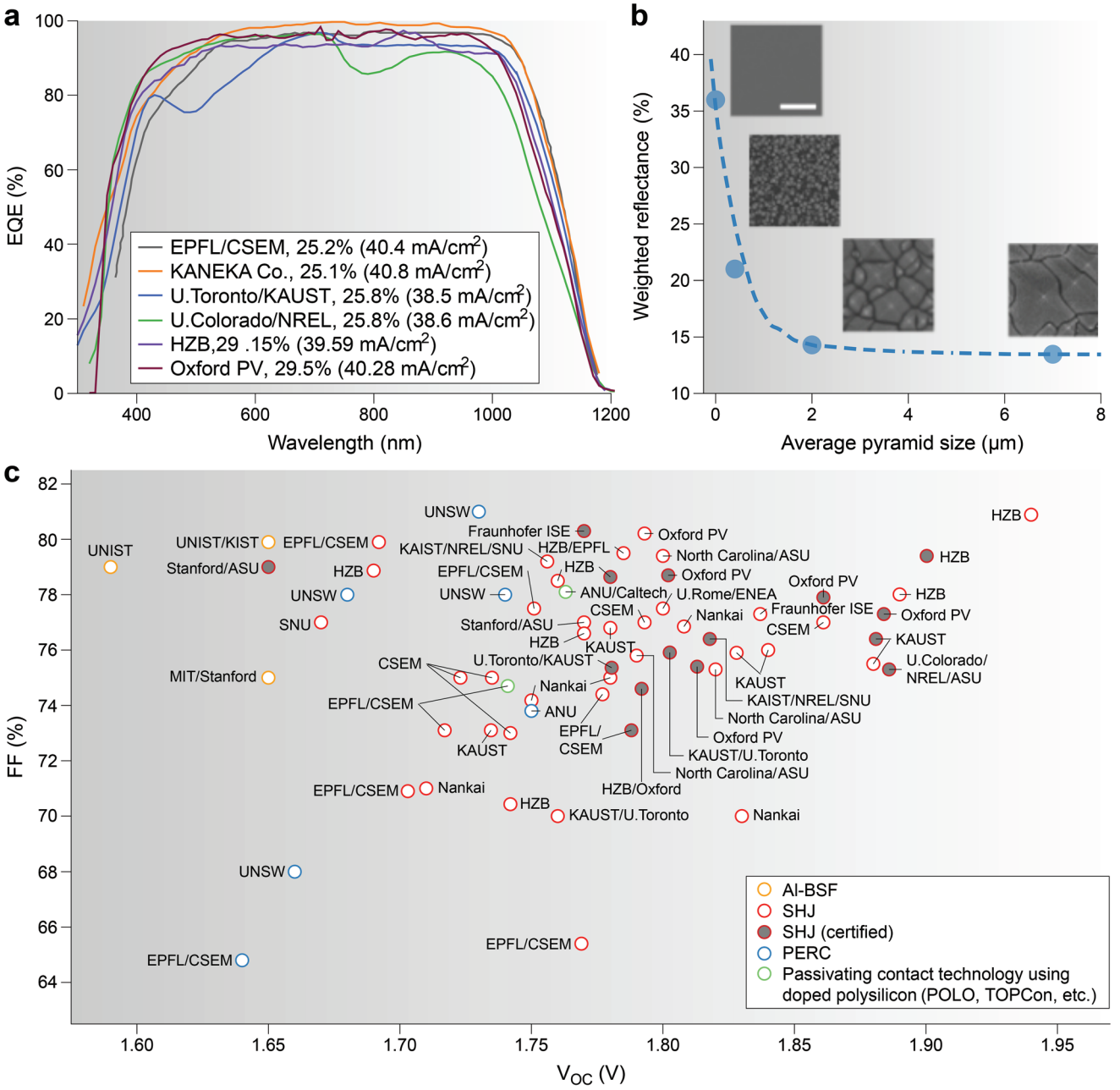

Figure 3. Optical and electrical performance of monolithic perovskite-silicon tandem solar cells. a) External quantum efficiency (EQE) of several representatives certified monolithic perovskite-silicon tandem devices. b) Measured weighted reflectance as a function of the pyramid size of c-Si (here the size of the pyramid base). SEM images of different textures are shown as insets (scale bar of 2 μm). c) FF as a function of V_{OC} for monolithic perovskite-silicon tandems reported so far. Yellow: Al back surface field (Al-BSF); blue: PERC; green: passivating contact; red: SHJ; open symbols: in-house measurements; solid symbols: independently certified values. b) Reproduced with permission.[66] Copyright 2020, The American Association for the Advancement of Science.

density integrated from EQE achieved by Sahli et al. reaches 40.4 mA cm^{-2} (excluding shadow losses induced by the front metal grid), a value approaching the J_{SC} of the cell of Kaneka (40.8 mA cm^{-2}, including shadow losses by the metal grid). As shown in Figure 3a, other tandem cell designs (flat with tuned recombination junction and/or textured antireflective foil on the front, textured with a non-conformal top cell, with or without an antireflective foil) all exhibit a lower EQE.

The higher EQE of conformally coated textured designs stems in part from lower reflection losses at the front side thanks to the enhanced probability of capturing light reflected at the sides of pyramid (transforming, e.g., a 10% reflection into a 1% one after a second bounce). It is worth noting that lowering the pyramid height from the standard ≈5 μm to about 1–2 μm to make this texture compatible with solution processing does not significantly increase reflectance at the wafer front surface

(Figure 3b). However, the flat surface of a solution-processed perovskite top cell deposited on textured c-Si will lead to some reflection losses as double bounce effects are absent at the front side. In any case, designs employing c-Si wafers textured on both sides, conformally coated or not, improve light trapping of infrared light compared to front side-polished tandems (Figure 3a).

Reflection at the interconnection junction should also be taken into account in the tandem design. The most widely employed recombination junctions are based on TCOs.[61–63,77–79] Due to a refractive index mismatch with c-Si, the TCO causes enhanced reflection at the sub-cell interface of light that should be absorbed in the c-Si. Replacing the TCO with nanocrystalline hydrogenated silicon (nc-Si: H) tunnel-junction reduces these reflection losses (as nc-Si: H has a refractive nearly identical to that of c-Si) and also parasitic absorption losses (as TCOs exhibit free carrier absorption at long wavelengths). Overall, 1 mA cm^{-2} is gained in the bottom cell by replacing the conventional TCO with an nc-Si:H recombination junction.[91,92] In addition to improving optical properties, this nc-Si: H tunnel-junction exhibits a lower conductance compared TCOs, which mitigates the impact of shunts that may be present in the top cell. An alternative option demonstrated by Mazzarella et al.[64] is to use a SiO_x multi-layer stack with finely tuned refractive indices to enhance light coupling into the c-Si cell.

Overall, when employing a conformally coated textured design, the margin for decreasing reflection losses and promote light trapping further is small compared to best-in-class SHJ cells. Further optical gains are more likely to result from lowering parasitic absorption, which primarily emerges from the front side charge carrier-selective layer, the buffer layer, and TCO. A careful choice of materials and thickness of the front contact and electrode stack will be essential to mitigate losses.[67] Noticeably, the 29.5% tandem cell of Oxford PV exhibits a low parasitic absorption of blue light compared to other cell designs. Regarding reported cell stacks, the C_{60} layer used as the electron contact at the front of p-i-n tandems is a noticeable source of parasitic absorption losses. There is however no alternative to this material in terms of performance at this stage of research. Parasitic absorption in the TCO can be mitigated by replacing ITO or indium zinc oxide layers conventionally used nowadays with higher mobility wider bandgap materials such as hydrogenated indium oxide or indium zirconium oxide.[93,95] Finally, screen-printing the Ag front grid instead of thermally evaporating it through a shadow mask (as done in most devices) will yield metal lines with a more favorable aspect ratio, hence lowering shadow losses.[83] Using SHJ single-junctions as a reference, by combining a c-Si wafer textured on both sides, a carefully optimized perovskite, and front electrode stack should enable tandems to achieve a J_{SC} of up to ≈20.5 mA cm^{-2} (including the shadow losses induced by the metal grid),[39,96,97] a value about 1 mA cm^{-2} higher than today's state-of-the-art.

3.2. V_{OC} and Fill Factor

Compared to the current density, there is currently more room to improve the V_{OC} and FF of tandem solar cells, especially for textured tandems, to surpass the 30% milestone. Figure 3c plots the FF versus V_{OC} of perovskite-silicon tandem solar cells reported so far. The FF of tandem devices employing a homojunction c-Si bottom cell is generally higher than when employing a SHJ bottom cell, while the opposite holds for V_{OC}. The V_{OC} of a tandem cell is the sum of each sub-cell V_{OC} at their corresponding illumination intensity and high V_{OC} bottom cells should be favored performance-wise (SHJs or cells based on high-temperature passivating contacts, which reach a V_{OC} of >720 mV under 1 sun conditions[98]). On the other hand, the correlation between the FF of the tandem cell and that of each sub-cell is not straightforward.[99] The loss of J_{SC} in a current mismatched tandem might lead to an improvement of FF of tandem cells. Based on the electrical simulations, Kohnen et al.[100] found that there is a dependency of the FF on the different current mismatching conditions and emphasized the need of applying power matching instead of the tranditional current matching.

As shown in Figure 3c, most of the perovskite-SHJ tandems have a V_{OC} below 1.85 V, with SHJs typically providing around 700 mV of V_{OC} (when high energy photons were absorbed by perovskite top cell and the light intensity for bottom silicon subcell was reduced roughly by half). The V_{OC} drops to 1.82 V or less for tandems that feature a c-Si wafer textured on both sides (1.79 V for conformally coated c-Si cells), highlighting the additional difficulty of covering the c-Si texture with a high-quality top cell. In that regard, the interconnection junction contacting the top and bottom cells may limit the impact of a lower quality top cell. The nc-Si:H recombination junction reported by Sahli et al.[75] exhibits a lower conductivity compared to TCOs, a lower conductivity that mitigates the impact of shunts that may be present in the top cell. This shunt quenching behavior is also beneficial when upscaling the device area (as a larger top cell is more likely to include local defects), as discussed below.

It is worth mentioning that most tandems reported at the early stage feature a top cell absorber with a bandgap (E_g) of 1.55 to 1.63 eV, materials primarily developed as perovskite single-junction solar cells. Indeed, mitigating voltage losses of perovskite materials featuring bandgaps theoretically more suitable for tandem applications (≈1.7 eV) remains a grand challenging task. For optimal performance with the 1.12 eV c-Si bottom cell, the bandgap of the perovskite top cell should be in the range from 1.65 to 1.73 eV when the operational temperature varies from 100 to 20 °C.[87] For <200 µm commercial Czochralski (CZ) silicon, the bandgap of the perovskite top cell should be widened to >1.7 eV,[85] which can be achieved by alloying iodide with bromide on the X site.[101,102] However, these wide-bandgap perovskites usually suffer from photoinduced halide phase segregation,[103] high trap density,[104] and likely ill-adapted charge selective contacts/interfaces,[104] leading to higher bandgap-to-V_{OC} losses ($W_{OC} = E_g/q - V_{OC}$, where q is the elementary charge) compared to lower bandgap materials.[105,106] The most promising strategies to mitigate these issues and boost properties further involve passivating bulk and interfacial defects.[107–109] The different approaches to do so include, amongst others, the addition of a small fraction of other elements to state-of-the-art $CsFAMAPb(I, Br)_3$ perovskite compositions to improve their photostability and material quality. In that regard, Xu et al.[67] found that incorporating Cl

stabilized 1.67 eV perovskites under illumination and improved photocarrier lifetime and carrier mobility by a factor of 2. By integrating such a triple-halide (Cl, Br, I) wide-bandgap perovskite with a SHJ bottom cell, a tandem efficiency of 27% was achieved thanks to a high V_{OC} of 1.89 V (W_{OC} of the top cell of 0.45 V).

Alternative options to lower the W_{OC} of the top cell include the use of donor-acceptor molecules as (part of) the charge carrier-selective contacts to passivate the absorber surfaces. Such an approach enabled reaching a W_{oc} of 0.45 V for a bandgap of 1.63 eV using a self-assembled monolayer (SAM) based on the carbazole moiety as the HTL,[110] or a W_{OC} of 0.43 V for a bandgap of 1.61 eV when using a fluorinated SAM on the ETL side.[111] Alternatively, the deposition of a high bandgap Ruddlesden-Popper perovskite on the perovskite surface leads to a W_{OC} as low as 0.41 V for a bandgap of 1.72 eV.[112,113] Partial substitution of A-site cations of $Cs_xFA_{1-x}PbI_yBr_{1-y}$ perovskites with the large dimethylammonium cation is an alternative strategy to slightly increase bandgap without introducing further phase segregation.[114,115] It has also been shown that perovskite lattice strain is directly linked to greater defect concentrations and non-radiative recombination, an effect that should be minimized by a suitable choice of processing parameters.[116,117]

We believe that double side texture design (include both industrial standard large pyramids and small pyramids) is the ultimate architecture to exploit the full efficiency potential of perovskite-silicon tandem solar cells. Currently, the main limitation in textured perovskite-silicon tandem solar cells is the low V_{OC} as compared to perovskite-silicon tandems grown on front polished wafers. This suggests significant non-radiative recombination loss in perovskite grown on the textured substrate. Another observation is that reducing the pyramid size generally yields better V_{OC}. This difference is most probably due to the difficulty of conformally coating the transport layer at the peak and valley of the pyramids. To further improve the quality of perovskite grown on a textured silicon substrate, future research should focus on 1) optimizing the optimal pyramid sizes, 2) developing a conformal coating of charge transport layers, 3) developing a conformal coating of surface passivation strategies.

Based on their optoelectronic properties, notably their sharp absorption edge,[118,119] perovskite solar cells should also achieve a W_{OC} < 0.4 V.[120,121] As a reference, best-in-class GaAs solar cells reach a W_{OC} of 0.29 V (for a bandgap of 1.42 V).[122] Assuming a realistic top cell V_{OC} of >1.26 V for a perovskite bandgap of 1.65–1.7 eV, the V_{OC} of tandem cells could be increased to >1.98 V provided that the SHJ bottom cell contributes 720 mV. It worth mention that V_{OC} of 1.94 V has already been demonstrated recently in a 29.2% monolithic perovskite-silicon tandem solar cell.[43] With a FF of 80%, a J_{SC} of 20.5 mA cm^{-2}, and a V_{OC} of 1.98 V, perovskite-SHJ tandems could realistically reach an efficiency of 32.5%, a value approaching that of record III–V on c-Si tandems.

4. Manufacturing of Large Area Tandem Cells and Modules

A critical factor that has enabled the rapid development of perovskite solar cells is their simple processability. Today, most perovskites are processed using the anti-solvent dripping spin coating method.[45,46] However, spin-coating is not ideal for high-throughput industrial manufacturing on 6-inch c-Si wafers, the standard wafer size used now by the c-Si industry. This chapter reviews alternative deposition protocols that are compatible with large-scale manufacturing.

Figure 4 compares efficiencies and cell sizes of monolithic perovskite-silicon tandem solar cells published in peer-reviewed journals and announced in press releases or at conferences until July 2021. A selection of perovskite, two-sides contacted SHJ, and IBC-SHJ single-junction solar cells are also included for comparison. Unlike c-Si cells, the efficiency of perovskite solar cells drops significantly when the cells' area are increased at this stage of research.[123,124] Small area (≈0.1 cm^2) perovskite solar cells prepared by spin-coating reach a certified efficiency of 25.7%.[44] This efficiency drops down to 20.1% and 17.9% when scaling up to 63.98 and 802 cm^2, respectively.[125]

With respect to perovskite-silicon tandems, Sahli et al.[92] reported in 2018 a 12.96 cm^2 perovskite-SHJ tandem cell, which reached an efficiency of 18% and employed an absorber processed by thermal evaporation/spin coating. Later, Zheng et al.[126] reported a 21.8% efficient perovskite-silicon homojunction cell with a perovskite spin-coated over an active area of 16 cm^2. In 2019, Kamino et al.[83] reported a stabilized efficiency of 22.6% (which was later increased to 24.4%) with a full 4-inch perovskite-SHJ tandem cell (active area of 57.4 cm^2) thanks to the use of a low-temperature screen-printed Ag metallization.[82] In 2021, several work on large arear tandems, where the perovskite absorbers were deposited by industrial scalable methods, were communicated at conferences/workshops. For example, HZB reported a 21.7% textured perovskite-silicon monolithic tandem cell with 60 cm^2 area where the perovskite is deposited by thermal co-evaporation (2021 tandemPV workshop). At 2021 MRS Fall Meeting, CSEM presented a 22.3%-efficient perovskite-silicon tandem (101.2cm^2) using blade coated perovskite absorber. Notably, an important upscaling milestone was achieved when Oxford PV announced a prototype 60 cell perovskite-silicon tandem module (PEROVSKITE-SI®: 435 Watt maximum power output, 23.5% module efficiency, and 25 years performance warranty) employing M6 size (a length of 166mm and a maximum diagonal length of 223mm) bottom cells at 2021 Industrialization of Perovskite Thin Film PV Technology workshop. While the tandem cell design, process flow, and efficiency were undisclosed, these results highlight the up-scalability of the technology to industry-relevant cell sizes. Below, we discuss a selection of perovskite deposition processes that may be employed to produce perovskite-silicon tandem cells featuring a 6-inch c-Si wafer.

4.1. Scalable Deposition Methods

The most common scalable methods for perovskite deposition can be categorized into 1) vapor-based techniques such as, thermal evaporation (physical vapor deposition) and chemical vapor deposition (CVD), and 2) solution-based routes, namely, blade-coating, slot-die coating, inkjet printing, spray-coating, etc., as reviewed by Li et al.[123] In **Figure 5**a, we highlight the cell efficiency as a function of the active area for a selection of perovskite single-junctions processed with these methods.

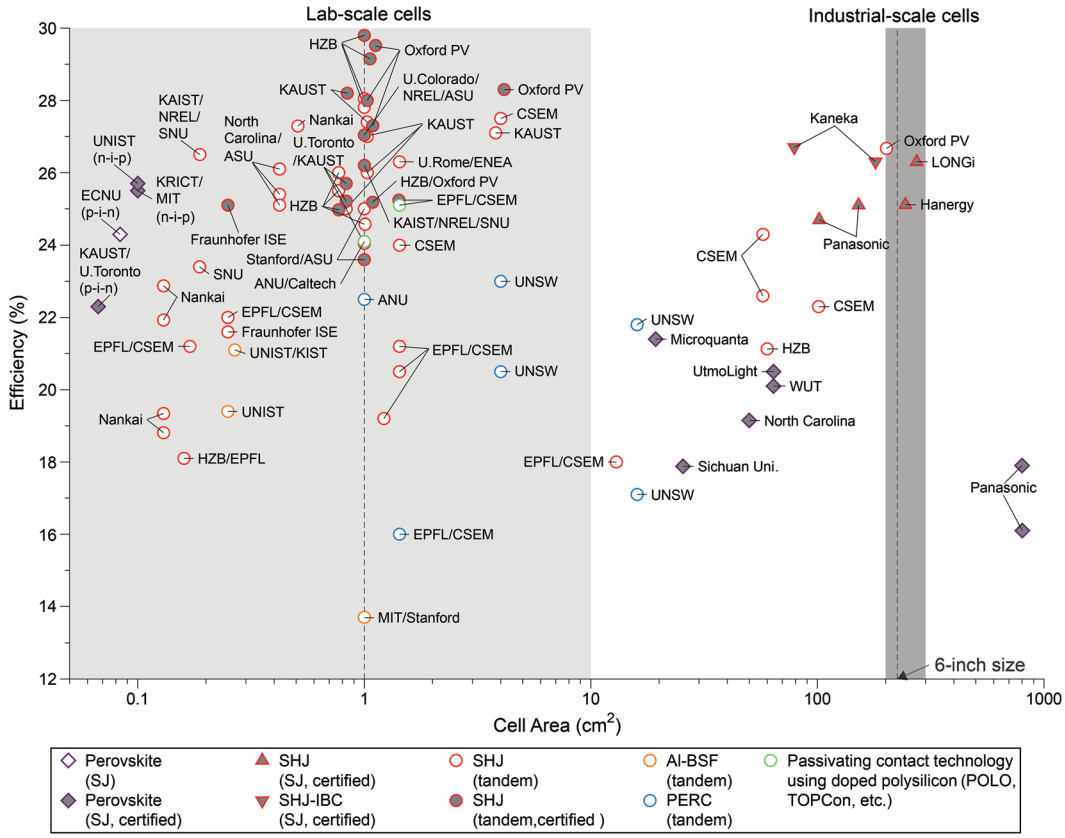

Figure 4. Up-scaling of monolithic perovskite-silicon tandem solar cells in comparison to single-junction technologies. Efficiencies of monolithic perovskite-silicon tandems, perovskite single-junction, and c-Si single-junction solar cells are plotted as a function of cell area. More details about the cells can be found in Table S1, Supporting Information. Diamond: perovskite single junction.[44,127,128] Upright and inverted triangle: certified double-side contact and interdigitated back contact (IBC) SHJ single junction.[17,19,91] Circle : perovskite/silicon tandem solar cell with different types of silicon bottom cell; yellow: Al back surface field (Al-BSF); blue: passivated emitter and rear contact (PERC); green: passivating contact technology using doped polysilicon; red: silicon heterojunction (SHJ); open symbols: in-house measurements; solid symbols: independently certified values.

4.1.1. Solution-Based Methods

Methods such as blade, inkjet, or slot die coating have recently emerged as a scalable high-throughput method for high-efficiency perovskite solar cells and modules. Figure 5b illustrates the blade-coating of a perovskite film, where a blade swipes the perovskite ink over the substrate. Usually, a nitrogen flow on the perovskite layer is used to accelerate the drying process (this is often referred to as gas quenching which is a desirable method that does not consume antisolvents and is compatible with large-area deposition methods[129–132]). The thickness of the perovskite layer can be tuned through the concentration of the perovskite precursor, the distance between the blade and the substrate, and the blade-coating speed. Since Deng et al.[133] reported the first blade-coated PSC with an efficiency of 15% in 2015, various strategies have been developed to improve the film uniformity over large areas, as well as, the devices' performance, for example, the engineering of compositions,[134] surfactants,[135] dopants,[136] additives,[137] and solvents.[138] The efficiency of small area (0.07 cm^2) blade-coated device has now reached 23.6% in a p-i-n configuration,[139] a value on par with record spin-coated p-i-n cells (24.3%, 0.096 cm^2).[127] Regarding upscaling, a certified module efficiency of 19.2% with an aperture area of 50 cm^2 and 18.2% with an aperture area of 30 cm^2 was achieved.[138,140] Importantly, the perovskite film was blade-coated at a speed of 99 mm s^{-1} at room temperature,[138] making the method attractive for high-throughput industrial manufacturing. In early 2020, this method was extended to tandems on c-Si. The HTL and the perovskite absorber were blade-coated directly on a SHJ cell featuring sub-micrometer pyramids on its front side, yielding a 26%-efficient tandem.[61]

Learnings from blade coating can be transferred to other scalable solution-based methods,[123,141,142] including slot-die-coating,[143,144] spray-coating,[145] inkjet printing,[146] etc., which have already achieved promising results at the single-junction level. While not necessarily yielding conformal perovskite coatings on c-Si pyramids, these deposition processes are still compatible with textured c-Si cells provided pyramidal features are downsized to about 1.5 µm or less.

4.1.2. Thermal Evaporation

Thermal evaporation is widely employed industrially to produce organic light-emitting diodes and thin-film solar cells (Cu(In, Ga)Se_2, CdTe, organic solar cells) and hence appears as an

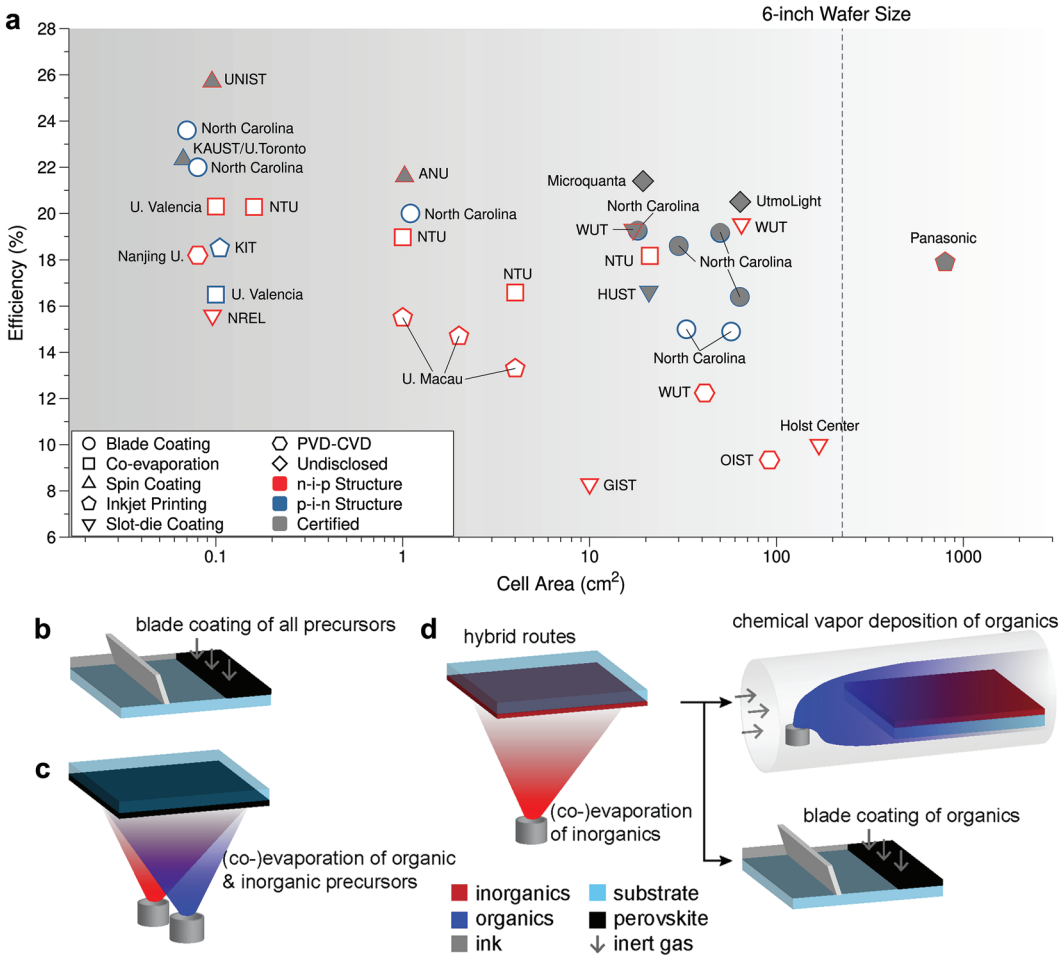

Figure 5. Scalable deposition methods for perovskites. a) Efficiency of single-junction perovskite solar cells and mini-modules prepared by industrially scalable methods. Perovskite solar cells prepared by spin coating are presented for comparison. Schematic drawings of a selection of industrially scalable perovskite deposition routes, such as, b) blade coating, c) co-evaporation, d) hybrid process. Spin-coated perovskite solar cells are included for comparison.

attractive method for perovskite deposition (Figure 5c). A comprehensive review of vapor phase deposited perovskite solar cells can be found elsewhere.[147–149] For tandems, the method yields conformal coatings on textured c-Si, enables precise control of layer thicknesses, involves low deposition temperatures, and is solvent-free. In addition to easing safety aspects, the absence of solvents widens the choice of charge carrier-selective layers deposited below the perovskite. The implementation of a thermally evaporated perovskite in a solar cell was first reported in 2013 by Liu et al.[150] They showed that uniform and compact $MAPbI_{3-x}Cl_x$ films could be obtained by co-evaporating MACl and PbI_2, enabling the demonstration of the first planar perovskite solar cells with an efficiency of 15.4%. Notable progress was made in 2016 by Momblona et al.[151] who demonstrated a fully evaporated planar perovskite solar cell with an efficiency above 20%. It is worth mentioning that the charge carrier-selective layers, the $MAPbI_3$ absorber, and the metal electrode were all sequentially evaporated, demonstrating, for the first time, an all vacuum-based process.[151] Importantly for tandems, they further showed that it is possible to tune the perovskite composition and hence its bandgap by co-evaporating from three[152] and even four[153] sources at the same time. Despite the demonstration of high efficiencies (>20%) on small area cells (≈0.16 cm^2) several years ago, larger cells (4 cm^2) and mini-modules (21 cm^2) based on co-evaporated perovskite solar cells were reported only recently.[154] Concerning tandems, several attempts have been made to deposit co-evaporated perovskite absorbers on textured c-Si substrates,[86,155–157] an efficiency of 24.6% was achieved recently.[86]

One issue with thermal evaporation is that, while inorganic cesium halide and lead halide salts evaporate in a ballistic way and their evaporation rate can be controlled by quartz crystal microbalances (QCMs), the evaporation of organic halide salts is more difficult to control due to their high vapor pressure under vacuum, low sticking coefficient on QCMs or chamber walls and varying sticking coefficient on different substrates.[158,159] To circumvent this issue, Mitzi and co-workers[160] developed a single-source flash evaporation technique to deposit a wide range of layered halide perovskites. A pre-synthesized perovskite material, for example, by a solution-based route, is placed on a metal heater in a vacuum and rapidly evaporated. In 2015, Bolink and co-workers[161] produced a 12.2%-efficient perovskite

solar cell featuring a flash evaporated $MAPbI_3$ absorber. Furthermore, large-area, uniform, and compact $MAPbI_3$ perovskite films with high crystallinity were demonstrated on 100 cm^2 area substrates with such a process route.[162] Considering the extremely short deposition time, single-source thermal evaporation is attractive from an industrial perspective as the composition of the perovskite may be easier to tune compared to multi-source co-evaporation.

4.1.3. Hybrid Routes

Blade-coating and other solution processing techniques usually involve toxic solvents,[163] such as, dimethylformamide, *N*-methyl-2-pyrrolidone, etc., while thermal evaporation often involves long deposition times and is complex to control when co-evaporating from multiple sources at the same time (e.g., to reach the desired bandgap for a tandem integration). These issues could be mitigated by separating the deposition of the inorganic precursors from that of the organic ones, tailoring each deposition step according to the requirements of each precursor. One demonstrated approach consists in depositing by thermal evaporation of an inorganic precursor layer composed of lead (PbI_2, $PbBr_2$, $PbICl_2$) and possibly cesium (CsI, CsBr, CsCl) halides, followed by its conversion to a perovskite phase by exposing it to an organohalide vapor or solution, as shown in Figure 5d. The perovskite composition can be tailored by manipulating the composition of the inorganic precursor layer and the organohalides. Notably, the hybrid thermal evaporation/spin-coating method[164,165] has been widely employed to produce efficient planar perovskite solar cells,[78,79,82,102,166] as well as, conformally coated textured tandems.[55,75] In view of upscaling the active area of the device, spin-coating can be upgraded to blade/slot-die coating (with the advantage over 1-step blade coating that organohalides do not require any toxic solvent as they dissolve in isopropanol or ethanol) or to a vapor-based method, for example, CVD. Concerning the latter, a hybrid PVD-CVD (thermal evaporation of PbI_2 and CsBr first, then conversion with FAI vapor) process flow has been used to fabricate 10×10 cm^2 perovskite mini-modules, reaching an efficiency of around 10%.[168] Very recently, Siegrist et al. reported the deposition of uniform perovskite layers deposited over 5 cm × 5 cm substrate area by combining thermal evaporation and blade coating. In conjunction with blade-coated charge transport layers, the champion perovskite solar cell that processed in ambient air using green solvents achieved power conversion efficiency up to 18.6%.[168]

Here we list several key parameters that should be considered when choosing which method to use for upscaling as shown in Table S3, Supporting Information. These parameters will all contribute to the cost of fabricating perovskite-silicon tandem solar cells, taking into account the efficiency, processing speed, and handling of toxic solvents, etc. In short, the solution-based method currently demonstrated the most efficient perovskite modules and could directly transfer most of the knowledge developed in the spin-coated method. However, the use of toxic solvent might increase the cost for protection and toxic solvent disposing of, etc. While the vacuum-based method does not involve any solvent and is suitable for conformal coating on a textured surface, it is challenging to tune the composition and implement passivation materials and additives that are essential for highly efficient and stable perovskite solar cells. As a compromise, the hybrid vacuum/solution method combines the conformal coating and the large chemical space for tuning composition. However, the main drawbacks are the incompatible processing schemes and the high Capital Expenditure. For more details about the different deposition approaches for perovskite, we refer the reader to the extensive review of the pros and cons of solution and vacuum-based methods by Vaynzof.[148]

4.2. Front-Side Metallization

A complication when up-scaling the active area to industry-relevant sizes comes from the need to modify the fabrication route of the front metal grid. Small-scale perovskite devices employ a thermally evaporated metal front grid through a mask, which leads to inefficient use of Ag (increasing costs) as well as, a low line conductance as the layer thickness remains thin (≈100 nm). As for c-Si single-junction cells, screen-printing appears as the deposition method of choice to metalize the front side of tandems as it leads to low line resistance without introducing significant shadow losses thanks to favorable finger aspect ratios (with fingers height reaching tens of µm). The thermal budget of metal halide perovskite top cells is limited to about 150 °C, a value lower than the temperature used to cure Ag pastes employed to metalize SHJ cells (about 200 °C). By optimizing the Ag paste composition, a sufficient bulk conductivity can be achieved after annealing <150 °C.[169] Thanks to these optimized Ag pastes, Kamino et al. demonstrated tandem devices that were screen-printed with a two-bus bar metallization design, achieving a steady-state efficiency of 22.6% (increased to 24.3%, as announced at the EU PVSEC 2019 conference) over an aperture area of 57.4 cm^2.[3,83] A drop in FF was observed when switching from evaporated Ag to screen-printed Ag, a loss that stems from an increase in contact resistance between the ITO and the screen-printed Ag paste. It is worth noting that this ITO/Ag paste contact resistivity may increase by up to 7 orders of magnitudes when lowering the curing temperature from 210 to 130 °C. Lowering contact resistance when screen-printing at low temperature will be essential to further improve the performance of large-area tandem devices. As an alternative to Ag screen-printing, Cu plating was recently demonstrated on perovskite single-junctions,[170] a method of high interest for the metallization of tandems, notably to reduce Ag consumption. A more detailed review on electrode metallization for scaled perovskite-silicon tandem solar cells could be found elsewhere.[171]

4.3. Module Integration

Literature concerning the integration of perovskite silicon tandems into modules remains scarce and has been discussing the impact of module design on hot spot temperature or 4-terminal designs.[172,173] At this stage, several aspects concerning cell sorting/binning, their interconnection, and encapsulation will need to be tackled to produce high-efficiency perovskite-silicon modules at high throughput. After processing, tandem cells will need to be sorted into groups exhibiting a similar

performance/photocurrent to avoid cell-to-cell current mismatch losses. In c-Si process lines, cell binning is typically achieved inline by flash testing each cell over 1 second or less, a measurement time that needs to remain short to maintain the high production throughput of 4000–10 000 cells h^{-1}.[4] A similar strategy applied to perovskite-silicon tandems is unlikely to yield precise measurements due to hysteresis and other dynamical effects (at least with the current set of materials).[174] The ion migration in perovskite solar cell is responsible for the current-voltage hysteresis and the slow *J*–*V* responses in perovskite solar cells. Although the maximum power point (MPP) tracking over some minutes is often applied in the laboratory to retrieve the steady-state performance of perovskite-based devices, there is no fast in-line diagnostic metrology for the quality control in in-line production.[175,176] The ionic nature of perovskite solar cells will probably require the development of dedicated industrial metrology protocols. Another critical aspect is the mechanical stability of the layer stack during the encapsulation process. Indeed, perovskite solar cells are particularly prone to delamination/fracture even under low mechanical loads.[177,178] In particular, failure often occurs first at the interface with the organic charge transport layers, layers that are common to most high-efficiency designs. This intrinsic instability of the technology to mechanical loads will require the development of novel processes for more robust module encapsulation. Concerning the encapsulation process itself, various protocols compatible with the thermal budget of perovskite solar cells (≈150 °C) have been reported, effectively suppressing extrinsic degradation pathways.[179–181] Overall, in spite of these challenges, industrialization efforts are on the way. Oxford PV MW pilot line is expected to deliver its first 6-inch perovskite-silicon tandem cells by 2022, with modules supposedly following soon after.[182]

5. Long-Term Stability

Perovskite-silicon tandems will certainly need to achieve operational stability comparable to that of c-Si cells to be commercially viable, i.e., they should still deliver 80% of their initial power output after 25 years in the field. Accelerated aging tests are often used to test the stability of various PV technologies. For c-Si PV, the International Electrotechnical Commission (IEC) has set a series of standard qualification tests (IEC 61215), which include mechanical, thermal, and environmental tests and often a specific limit of degradation allowed after each test.[183] While some perovskite-based single-junction devices now pass some of these tests, that is, tests involving damp heat (encapsulated, 1000 h at 85 °C in 85% relative humidity),[80] thermal cycling (encapsulated, 200 cycles from –40 to 85 °C),[184] humidity freeze (50 thermal cycles, then 10 cycles –40 to 85 °C in 85% relative humidity),[185] a 25 year lifetime is not guaranteed due to the specific degradation modes of perovskites. Adaptations to these established IEC standards are certainly required for perovskite-based devices to account for the peculiar ionic properties of perovskites. In that regard, a consensus has recently been reached to employ test protocols based on the International Summit on Organic Photovoltaic Stability (ISOS) procedures.[186] The paragraphs below will discuss a small selection of intrinsic stability issues that perovskite-based tandems are facing (**Figure 6**a), as well as some mitigation strategies (Figure 6b). Extrinsic degradation pathways will not be covered here in great detail as these should be effectively suppressed by the encapsulation. The latest progress on general perovskite solar cell stability, current understanding of degradation mechanisms, field-testing, and strategies to address them can be found elsewhere.[187–191]

5.1. Current Stability Status of Perovskite-Silicon Tandems

So far, only a few studies have investigated the stability of monolithic perovskite-silicon tandem solar cells over the long term. Encapsulated tandem devices typically retain ≈90% of their initial efficiency after 250 h of operation at MPP under continuous one sun illumination.[61,65,75] Hou et al.[66] demonstrated encapsulated devices that maintained their original performance after 400 h at 85 °C in the dark and after 400 h of operation at MPP at 40 °C, in both cases in ≈40–50% relative humidity. Al-Ashouri et al.[43] showed that unencapsulated devices maintained 95% of their initial efficiency after 300 h long-term MPP track using a dichromatic LED illumination in the ambient air at a controlled temperature of 25 °C and relative humidity of 30 to 40%. De Bastiani et al. investigated the outdoor stability of perovskite/silicon tandems over six months. While a degradation linked to the perovskite absorber was found to be reversible at night, the metal electrode irreversibly reacted with iodine, leading to a loss in FF from about 80% to 50%.[192] Although these preliminary results are encouraging, significant efforts are required to bring the stability of tandem solar cells to a level that is comparable to c-Si bottom cells, which typically demonstrate 80% or more of their initial performance after 25 years in the field (corresponding to ≈50,000 h of sunlight).

5.2. Perovskite Absorber Decomposition upon Various Stress Factors (Heat, Light, Moisture, Bias, etc.)

One issue of particular importance is that perovskite absorbers can decompose when exposed to some of their constituent elements.[193] Indeed, Wang et al. found that perovskite films ($MAPbI_3$, $FAPbI_3$, $FA_{0.8}CsPbI_3$) can severely degrade when exposed to an I_2 vapor, leading to a further release of I_2 sustaining an autocatalytic degradation pathway.[194] I_2 was found to be generated in perovskite solar cells under operational conditions at 80 °C,[195] initiating degradation within perovskite grains (Figure 6a). Residual PbI_2, which is often added on purpose as it is beneficial efficiency-wise, was found to decompose into I_2 and metallic Pb upon illumination and may have acted as the initial source of I_2.[195] As I_2 volatilization may be difficult to completely suppress, mitigation strategies should be developed. Wang et al. introduced a pair of europium ions of Eu^{3+}-Eu^{2+}, which can selectively oxidize metallic Pb and reduce I_0 defects, improving long-term operational stability.[196] Recently, Lin et al. found that ionic liquids, such as a piperidinium salt additive could retard both segregations into impurity phases and pinhole formation upon aging.[197]

Moisture ingress may also lead to a decomposition of the perovskite absorber. While encapsulation should avoid such extrinsic degradation,[185] thin buffer layers may add an extra level of protection (Figure 6b). Yang et al.[198] deposited a dense

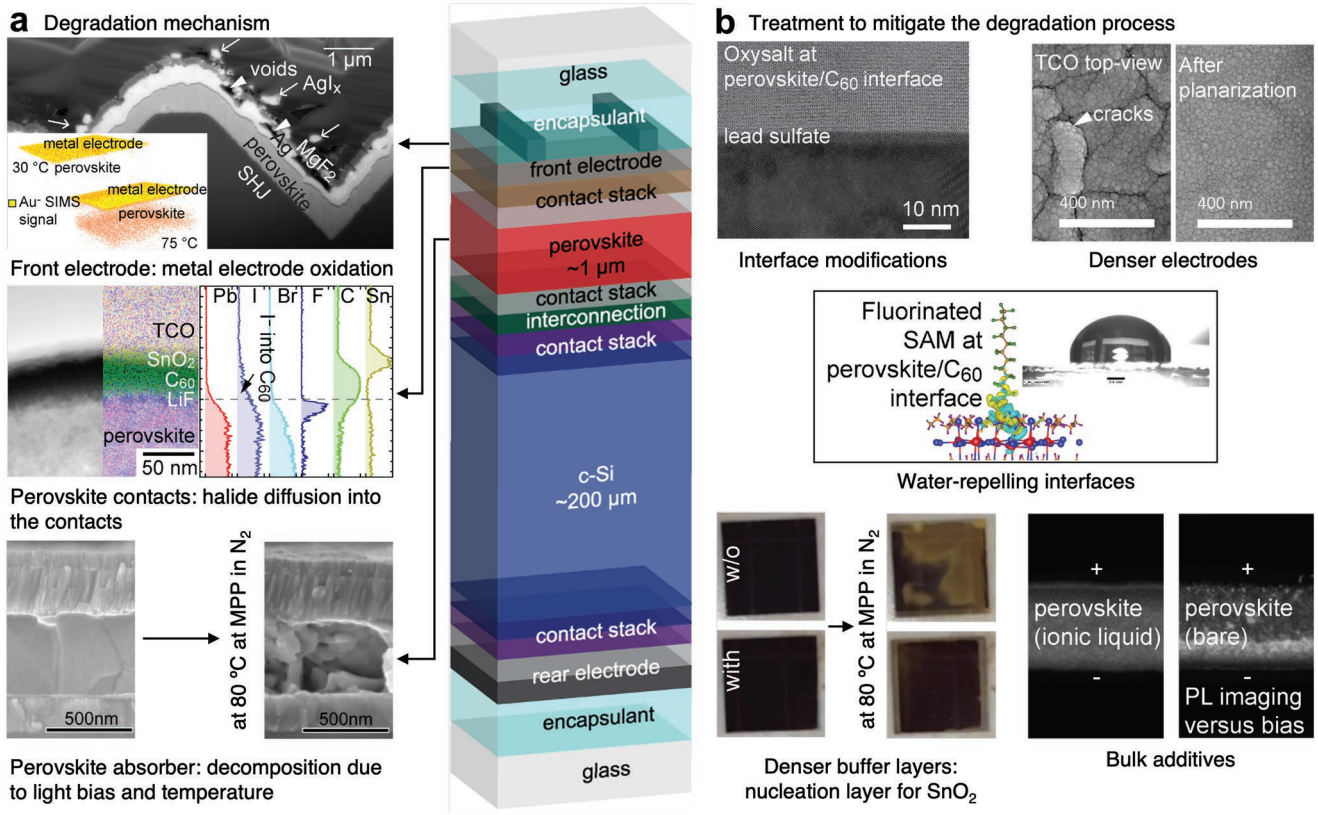

Figure 6. Summary of a selection of degradation mechanisms of perovskite solar cells and mitigation strategies. a) Degradation mechanisms of perovskite solar cells: Front electrode degradation, for example, the oxidation or migration of the metal contact from the front electrode;[193] charge transport layer degradation, for example, iodide migration into C_{60} during partial shading;[200] perovskite absorber degradation, for example, its decomposition upon long-term stability testing at temperatures on the order of 80 °C due to I_2 vapor release.[195] b) Common mitigation strategies for the degradation process: Surface modifications for improved stability (oxysalt[198] or perfluorinated[111] compounds at the perovskite/C_{60} interface), or nucleation layers that promote the growth of denser barrier layers (buffer or TCO);[199,201] bulk additives (ionic liquids[202]) to retard the absorber degradation. a) Left bottom image: Reproduced with permission.[195] Copyright 2019, Royal Society of Chemistry, left middle image: Reproduced with permission.[200] Copyright 2019, Royal Society of Chemistry, left top image: Reproduced with permission.[75] Copyright 2018, Springer Nature, left top (inset): Reproduced with permission.[203] Copyright 2016, American Chemical Society. b) Top left: Reproduced with permission.[198] Copyright 2019, The American Association for the Advancement of Science, middle: Reproduced with permission.[111] Copyright 2020, American Chemical Society, top right: Reproduced with permission.[201] Copyright 2020, American Chemical Society, and bottom left: Reproduced with permission.[189] Copyright 2019, Wiley-VCH Verlag GmbH & Co. KGaA, Weinheim, bottom right: Reproduced with permission.[204] Copyright 2019, Springer Nature.

layer of lead oxysalt on the perovskite surface, which provided enhanced water resistance. The layer was found to bind with undercoordinated lead defects lowering the number of defect nucleation sites on the surface. Their encapsulated devices maintained about 97% of the initial efficiency after 1200 h MPP operation at a realistic operation temperature of 65 °C. Alternatively, Raiford et al. demonstrated that enhancing the nucleation of the SnO_2 buffer deposited by ALD through the functionalization of the C_{60} surface via polyethylenimine ethoxylated, leading to improved moisture and thermal stability.[199] Also, the deposition of a water-repelling fluorinated SAM at the perovskite/C_{60} interface resulted in devices that remained stable during 250 h at 85 °C in N_2 at MPP.[111]

5.3. Ion Migration

The ionic nature of perovskite solar cells and low activation energy for ion migration pose severe stability concerns.[205,206] Detrimental chemical reactions associated with ion migration and ion accumulation/reaction in/with neighboring charge carrier-selective layers have been frequently reported (Figure 6a).[207,208] While inherent to this class of materials, ion migration should be mitigated and contained to the perovskite absorber to avoid accelerated degradation. In that regard, ion migration can be attenuated by either reducing the mobile ion density,[209,210] and/or the number of ion migration channels,[205,211,212] as well as, increasing the ion migration barrier.[213] With respect to high bandgap materials, phase segregation upon illumination highlights the high mobile ion density. Abdi-Jalebi et al. showed that ion migration and phase segregation could be substantially mitigated by decorating the perovskite surface and grain boundaries with potassium halides that are not incorporated into the perovskite lattice.[210] Using a triple halide (Cl, Br, I) perovskite composition, Xu et al.[67] substantially improved the photostability of the perovskite with bandgap = 1.67 eV. Alternatively, introducing phenethylammonium-based 2D additives along with mixed anions thiocyanates (SCN), Kim et al.

demonstrated 1.7 eV perovskites with excellent photostability.[68] The addition of a small amount of ionic liquids[202] within the perovskite absorber has been shown to reduce the number of defects and mobile ionic species (Figure 6b), leading to devices exhibiting little degradation upon light illumination at 70–75 °C for over 1000 h when encapsulated.[204] The use of surface-anchoring alkylamine ligands was also shown to reduce the density of traps and ion migration, leading to 22.3%-efficient p-i-n single-junction cells stable for 1000 h at MPP at 40 °C under UV-filtered light.[128] Using surface treatment with molecules containing both electron-rich and electron-poor moieties, such as phenformin hydrochloride (PhenHCl), Isikgor et al showed 1.68 eV devices without any V_{OC} losses after more than 3000 h of thermal stress at 85 °C in a nitrogen atmosphere.[88]

5.4. Metal Electrode Degradation

Commercially available c-Si solar cells use Ag as the front grid. Ag can react with the iodine of the perovskite, leading to performance degradation.[214] Ag oxidation was observed at both the front and rear sides of the textured monolithic perovskite-SHJ tandem solar cell after 250 h of stability testing (glass/glass with edge sealant but no encapsulant, Figure 6a) and after 6 months in the field.[75,192] The Ag oxidation on the rear side of the tandem cell suggests that some iodide transport may have occurred in the form of volatile species during operation. Alternatively, metals may also diffuse into the absorber during operation and degrade it (Figure 6a).[203,215,216] Avoiding the rapid oxidation of the metallization as well as the migration of metal into the absorber will certainly require the development of dense diffusion barriers (Cr_2O_3,[217] SnO_2[199]). In that regard, planarizing the perovskite surface prior to the deposition of the TCO layer was shown to inhibit the permeability of the latter to metal migration (Figure 6b).[201]

5.5. Other Field Operation Effects

Partial shading induced by a neighboring tree or building or during cleaning may lead to permanent degradation of PV modules. As cells are connected in series, when the operating current exceeds the J_{sc} of a shaded cell or faulty cell, such cell will be forced into reverse bias condition. As it can cause local overheating, the hot spots will occur in the solar cells, which could lead to the formation of hot spots in the shaded cell if faulty (leading, e.g., to local temperatures >100 °C in c-Si modules).[218,219] Several studies investigated the reverse bias stability of perovskite single-junction solar cells.[200,220–222] The application of a reverse bias voltage resulted in both reversible and irreversible performance changes, with metallized single-junctions being particularly prone to the latter (unlike cells, e.g., featuring a carbon electrode[223]). Reversible changes were triggered notably by ionic migration, for example, in the form of iodide into the C_{60} charge carrier-selective contact (Figure 6a), while irreversible ones were induced by the formation of shunts. Deng et al. investigated the partial shading resilience of mini-modules by shading one sub-cell while keeping all other segments under 1-Sun illumination. It took 2 to 4 min for the shaded sub-cell to reach breakdown conditions under MPP tracking. The mini-module performance decreased from 15.7% to 15.1% after >50 cycles of shading/de-shading on the same sub-cell of a mini-module. The effect of partially shading 2-terminal (and 4-terminal) tandem modules has also been investigated through simulations.[172] Several options to lower hot spot temperature were discussed, notably the use of IBC bottom cells or by adding a number of bypass diodes.

Other modes of degradation may occur in the field, for example, ultraviolet (UV) induced degradation and potential induced degradation (PID). Parasitic UV absorption by the top carrier transport layer in perovskite solar cells will cause UV-induced degradation in perovskite solar cells[223,224] and perovskite-Si tandems.[225] Strategies such as using an UV blocker in the encapsulant or even applying a down-shift material on the top of perovskite solar cells have been shown to effectively suppress UV-induced degradation.[224,225] At the end of the module string, the voltage difference between the cell and the frame or metallic support can be as high as 1500 V, which can lead to PID. Na^+ ions from the glass may migrate to the c-Si cell depending on the choice of packaging materials, triggering irreversible degradation of thin film and c-Si PV technologies.[226–229] In addition, the TCO layer of SHJ cells has been shown to decompose into In-rich clusters due to PID.[226–228] High bulk resistivity encapsulants will certainly be needed to avoid PID in tandems. Various strategies at the cell and module can be taken to prevent PID, notably by using encapsulant materials with high bulk electrical resistivity (e.g., an ionomer with a volume resistivity of around 10^{16} Ω cm instead of an ethylene-vinyl acetate (EVA) with 10^{14} Ω cm[228]) and an edge sealant to prevent water ingress (the latter reduces the electrical resistivity of the encapsulant). At equal potential difference, increasing the encapsulant bulk electrical resistivity reduces the electronic and ionic leakage currents flowing from the frame to the cells, or vice-versa.

To conclude on stability aspects, perovskite-based devices are becoming more and more stable and now pass several important IEC tests but the road to a 25 years-stable product is still long and uncertain. Intrinsic degradation processes, that is, ionic migration or perovskite decomposition when exposed to some of its volatile elements, will need to be tackled. And similarly to light and elevated temperature-induced degradation occurring in PERC cells,[231,232] operations in the field of the first perovskite(-silicon) tandem modules will certainly reveal additional degradation pathways not anticipated in the laboratory.[233,234]

6. Other Monolithic Tandem Cell Designs

6.1. Bifacial Tandems

Bifacial cells can harvest photons from both the front and rear sides, leading to increased energy yield compared to monofacial cells.[235,236] The International Technology Roadmap for Photovoltaic predicts an 80% market share for c-Si bifacial cell technologies by 2030.[4] Advantageously, PERC, TOPCon, and SHJ cells can be made bifacial provided the rear metallization is adapted, with SHJs exhibiting the highest bifaciality (>95%).[237] The advent of bifacial single-junction c-Si cells certainly raises

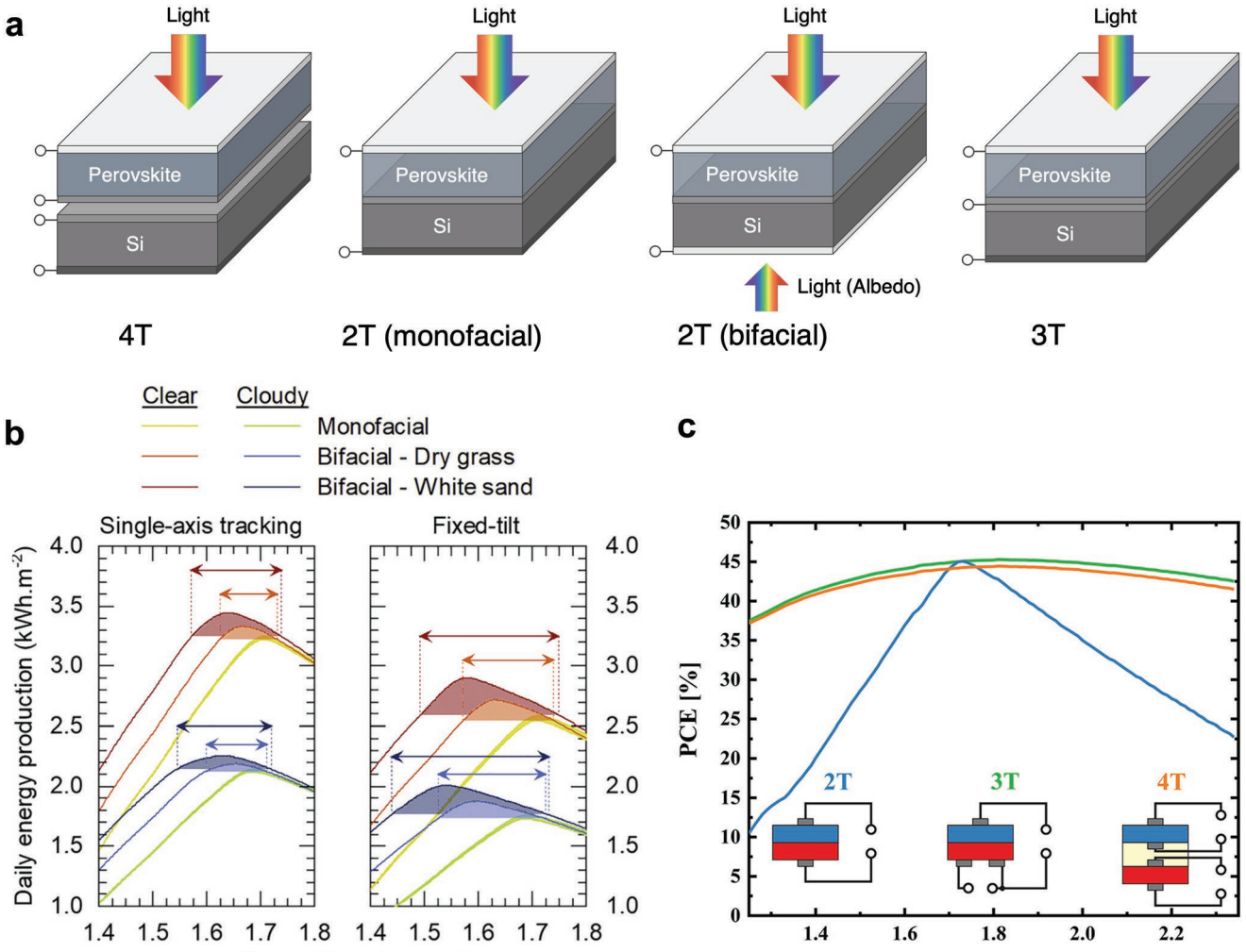

Figure 7. Bifacial and 3-terminal perovskite-IBC tandem solar cells. a) Roadmap for the research on perovskite/silicon dual-junction tandem cell. b) Energy produced daily for different mono facial and bifacial tandem designs for two ground types (single-axis tracking configuration). c) Simulated efficiency of 2-, 3-, and 4-terminal mono facial tandems depending on the perovskite top cell bandgap, highlighting the absence of current mismatch losses for the last two designs. b) Reproduced with permission.[243] Copyright 2020, Elsevier Inc. c) Reproduced with permission.[245] Copyright 2020, American Chemical Society.

the efficiency threshold that must be achieved by tandems to enter the market. However, tandems may also benefit from harvesting rear illumination, as demonstrated by various theoretical and experimental studies **Figure 7**b).[236,238–244] A key aspect to benefit from bifaciality is to alter the design of the top cell so that the device operates close to current matching conditions with rear illumination. The top cell needs to absorb more photons compared to its monofacial equivalent as the rear illumination is absorbed solely in the bottom cell, meaning that the perovskite bandgap should be lowered (from 1.7 eV to, e.g., 1.6–1.5 eV). While the exact gain provided by bifaciality depends on many parameters (location, ground albedo, front and rear illumination spectrum, current mismatch, module mounting configuration, array configuration, temperature, etc.), bifacial tandems may produce about 20% more energy yield than bifacial c-Si single-junctions in the best-case scenario (solitary array, no ground shading).[242,244] Another advantage is that bifaciality widens the choice of top cell bandgap (Figure 7b).[236,243]

6.2. 3-Terminal Tandems

The use of an IBC bottom cell or an intermediate transparent conductive electrode between the two sub-cells enables the production of a monolithic 3-terminal tandem, a cell design not prone to sub-cell current mismatch losses as shown in Figure 7c. While the first 3-terminal perovskite-silicon devices are starting to emerge,[245,246] similar designs have been demonstrated in the past using III–V materials on silicon or other materials combinations, as reviewed in ref. [247]. Amongst the different options to make a 3-terminal cell, the use of an IBC c-Si cell certainly appears as the most promising to avoid the parasitic absorption losses and resistive losses induced by the intermediate electrode. The presence of the third terminal at the back of the IBC 3-terminal tandem design eliminates the need for current matching and offers a significant degree of flexibility when designing the perovskite top cell. But this additional level of flexibility comes at the expense of system costs

as extra wires and electronics are needed to maintain the cell at MPP compared to a 2-terminal design and module integration is made more complex.[248]

7. Lead Management and Cycling

To further remove the barrier of the commercialization of perovskite solar cells, the toxicity of lead that exists in the most efficient metal halide perovskite must be considered. There are mainly two strategies to solve the problem, I) preventing lead leakage from the working modules and II) recycling lead from the decommissioned modules. Regarding the reduction of lead leakage, Jiang et al.[249] demonstrated that using an epoxy resin for encapsulation can reduce the Pb leakage rate by a factor of 375 compared with using a glass cover with a UV-cured resin. Li et al.[250] developed a Scotch-tape-like design of EVA film and a pre-laminated P,P'-di(2-ethylhexyl)methanediphosphonic acid layer that can capture over 99.9% of Pb leakage from the damaged PSCs by applying it on both sides of the cells. Chen et al.[251] used a cation-exchange resin-based method that can prevent lead leakage from damaged perovskite solar modules. Meanwhile, the same group[252] integrated a mesoporous sulfonic acid-based lead-adsorbing resin into perovskites, demonstrating more effectiveness in preventing lead leakage than the configuration with the coating on the glass surface. On the other hand, Chen et al.[253] reported a lead management method for perovskite solar modules with a recycling efficiency of 99.2%, in which lead is first separated by weakly acidic cation exchange resin and is released as soluble $Pb(NO_3)_2$, then followed by precipitation as PbI_2. Park et al.[254] reported a new adsorbent, iron-incorporated hydroxyapatite, for both separation and recovery of Pb from PSCs, which guarantee recycling of 99.97% of Pb ions by forming lead iodide.

8. Conclusions and Outlook

A technological upgrade is occurring in the field of c-Si PV, with more efficient designs quickly replacing older less efficient ones to drive down costs. With the practical PCE limit of c-Si of ≈27% approached at the R&D level, upgrading c-Si with a perovskite top cell to form a monolithic 2-terminal tandem certainly appears today as one of the most promising avenues to continue the learning curve of c-Si over the long term. Indeed, the possibility of refurbishing existing c-Si process flows with a few extra perovskite deposition steps to reach efficiencies >32% makes this tandem technology well suited for a rapid industrial implementation strategy. As reviewed here, results obtained in just a few years of R&D certainly start to confirm this potential.

This review first discussed the current status of 2-terminal monolithic perovskite-silicon tandems, notably bottom cell c-Si technologies most suited for a tandem integration as well as perovskite top cell designs that maximize performance and compatibility with the bottom cell. In that regard, the demonstration of perovskite deposition processes that are directly compatible with the front-side texture of c-Si certainly appears to be an important step. With the efficiency of lab-scale devices approaching the 30% mark, the main aspects discussed here focused on the up-scalability to industry-relevant devices areas (from 1×1 to 6×6 square inches), module integration as well as long-term operational stability. Despite rapid progress—lab-scale devices now start to pass IEC tests—long-term stability is still the main issue hindering perovskite PV. Similar stability to c-Si appears to be needed to ensure the commercial viability of perovskite-silicon modules for utility-scale or rooftop applications (i.e., 25 years of warranty in the field). Several pathways to improve stability (without affecting performance) were discussed.

Alternative monolithic tandem designs were also reviewed, for example, bifacial tandems, where light reaching the rear of the device contributes to increasing the overall photocurrent and hence performance, as well as, 3-terminal devices employing an IBC bottom device to avoid current mismatch losses. The continuous need to improve efficiencies further may also lead to triple-junction perovskite-perovskite-silicon solar cells,[102] a type of device that may displace 2-terminal tandems on the long-term, provided that the device complexity, current-mismatch losses, or any other issues do not then become a barrier to their effectiveness as a commercial photovoltaic product.

Finally, given the fact that it has taken decades of research and development for c-Si technologies to achieve the level of success they enjoy today, it is promising to witness the rapid progression of perovskite-silicon tandem solar cells and first commercial perovskite-c-Si modules may not be too far ahead.

Supporting Information

Supporting Information is available from the Wiley Online Library or from the author.

Acknowledgements

Y.H. acknowledges the support from the National University of Singapore (NUS) Presidential Young Professorship (R-279-000-617-133 and R-279-001-617-133). This work was authored in part by SERIS, a research institute at the NUS. SERIS was supported by NUS, the National Research Foundation Singapore (NRF), the Energy Market Authority of Singapore (EMA), and the Singapore Economic Development Board (EDB). This work was supported by funding from the Swiss Federal Office of Energy (SFOE)-BFE (projects No.: SI/501805-01 and SI/501804-01) and the Swiss National Science Foundation (SNF)-Bridge (projects No.: 20B2-1_176552/1 and CRSII5_171000). T.C.-J.Y. would like to acknowledge the support of the EU Horizon 2020 Marie Skłodowska-Curie Individual Fellowship under grant "POSITS" (No. 747221) as well as, the CSIRO Research Office for project funding and fellowship support.

Open access funding provided by ETH-Bereich Forschungsanstalten.

Conflict of Interest

The authors declare no conflict of interest.

Author Contributions

F.F. and Y.H.: Concept and original idea behind this article; F.F.: Writing—Original draft, with the help of Q.J.; F.F., J.L., H.L., T.C., J.Y., Q.J., Y.H.: Writing—Manuscript revision; F.F., J.L., H.L., T.C., J.Y., Y.H., A.F., Q.J., and C.B.: Writing—Review, discussion, and editing; Q.J., C.B., and Y.H.: Supervision.

Keywords

high efficiency, perovskite solar cells, perovskite-silicon tandem solar cells, stability, upscaling

Received: August 19, 2021
Revised: November 17, 2021
Published online: April 7, 2022

[1] International Energy Agency, *Global Energy Review*, **2020**, *2020*, https://www.iea.org/reports/global-energy-review-2020.
[2] V. Sivaram, S. Kann, *Nat. Energy* **2016**, *1*, 16036.
[3] E. Bullich-Massagué, F.-J. Cifuentes-García, I. Glenny-Crende, M. Cheah-Mañé, M. Aragüés-Peñalba, F. Díaz-González, O. Gomis-Bellmunt, *Appl. Energy* **2020**, *274*, 115213.
[4] International Technology Roadmap for Photovoltaic (ITRPV) **2020**.
[5] C. Battaglia, A. Cuevas, S. De Wolf, *Energy Environ. Sci.* **2016**, *9*, 1552.
[6] D. M. Powell, M. T. Winkler, H. Choi, C. B. Simmons, D. B. Needleman, T. Buonassisi, *Energy Environ. Sci.* **2012**, *5*, 5874.
[7] I. M. Peters, C. D. R. Gallegos, S. E. Sofia, T. Buonassisi, *Joule* **2019**, *3*, 2732.
[8] M. A. Green, *Nat. Energy* **2016**, *1*, 15015.
[9] M. A. Green, *Joule* **2019**, *3*, 631.
[10] M. A. Green, *Sol. Energy Mater. Sol. Cells* **2015**, *143*, 190.
[11] T. Dullweber, J. Schmidt, *IEEE J. Photovoltaics* **2016**, *6*, 1366.
[12] A. Blakers, *IEEE J. Photovoltaics* **2019**, *9*, 629.
[13] A. Richter, J. Benick, F. Feldmann, A. Fell, M. Hermle, S. W. Glunz, *Sol. Energy Mater. Sol. Cells* **2017**, *173*, 96.
[14] A. Rohatgi, B. Rounsaville, Y.-W. Ok, A. M. Tam, F. Zimbardi, A. D. Upadhyaya, Y. Tao, K. Madani, A. Richter, J. Benick, *IEEE J. Photovoltaics* **2017**, *7*, 1236.
[15] B. Kafle, B. S. Goraya, S. Mack, F. Feldmann, S. Nold, J. Rentsch, *Sol. Energy Mater. Sol. Cells* **2021**, *227*, 111100.
[16] C. Hollemann, F. Haase, M. Rienäcker, V. Barnscheidt, J. Krügener, N. Folchert, R. Brendel, S. Richter, S. Großer, E. Sauter, J. Hübner, M. Oestreich, R. Peibst, *Sci. Rep.* **2020**, *10*, 658.
[17] D. Adachi, J. L. Hernández, K. Yamamoto, *Appl. Phys. Lett.* **2015**, *107*, 233506.
[18] D. D. Smith, P. Cousins, S. Westerberg, R. De Jesus-Tabajonda, G. Aniero, Y.-C. Shen, *IEEE J. Photovoltaics* **2014**, *4*, 1465.
[19] K. Yoshikawa, H. Kawasaki, W. Yoshida, T. Irie, K. Konishi, K. Nakano, T. Uto, D. Adachi, M. Kanematsu, H. Uzu, K. Yamamoto, *Nat. Energy* **2017**, *2*, 17032.
[20] A. Richter, M. Hermle, S. W. Glunz, *IEEE J. Photovoltaics* **2013**, *3*, 1184.
[21] S. Schäfer, R. Brendel, *IEEE J. Photovoltaics* **2018**, *8*, 1156.
[22] L. C. Hirst, N. J. Ekins-Daukes, *Prog. Photovoltaics* **2011**, *19*, 286.
[23] R. K. Kothandaraman, Y. Jiang, T. Feurer, A. N. Tiwari, F. Fu, *Small Methods* **2020**, *4*, 2000395.
[24] M. H. Futscher, B. Ehrler, *ACS Energy Lett.* **2016**, *1*, 863.
[25] S. Essig, C. Allebé, T. Remo, J. F. Geisz, M. A. Steiner, K. Horowitz, L. Barraud, J. S. Ward, M. Schnabel, A. Descoeudres, D. L. Young, M. Woodhouse, M. Despeisse, C. Ballif, A. Tamboli, *Nat. Energy* **2017**, *2*, 17144.
[26] R. Cariou, J. Benick, F. Feldmann, O. Höhn, H. Hauser, P. Beutel, N. Razek, M. Wimplinger, B. Bläsi, D. Lackner, *Nat. Energy* **2018**, *3*, 326.
[27] J. C. Goldschmidt, L. Wagner, R. Pietzcker, L. Friedrich, *Energy Environ. Sci.* **2021**, *14*, 5147.
[28] 2020 Final report: Study on the EU's list of critical raw materials, https://ec.europa.eu/growth/sectors/raw-materials/areas-specific-interest/critical-raw-materials_en.
[29] G. E. Eperon, S. D. Stranks, C. Menelaou, M. B. Johnston, L. M. Herz, H. J. Snaith, *Energy Environ. Sci.* **2014**, *7*, 982.
[30] H. Min, D. Y. Lee, J. Kim, G. Kim, K. S. Lee, J. Kim, M. J. Paik, Y. K. Kim, K. S. Kim, M. G. Kim, T. J. Shin, S. Il Seok, *Nature* **2021**, *598*, 444.
[31] W.-J. Yin, T. Shi, Y. J. A. P. L. Yan, *Appl. Phys. Lett.* **2014**, *104*, 063903.
[32] Q. A. Akkerman, G. Rainò, M. V. Kovalenko, L. Manna, *Nat. Mater.* **2018**, *17*, 394.
[33] T. Leijtens, K. A. Bush, R. Prasanna, M. D. McGehee, *Nat. Energy* **2018**, *3*, 828.
[34] M. Anaya, G. Lozano, M. E. Calvo, H. Míguez, *Joule* **2017**, *1*, 769.
[35] J. Werner, B. Niesen, C. Ballif, *Adv. Mater. Interfaces* **2018**, *5*, 1700731.
[36] G. E. Eperon, M. T. Hörantner, H. J. Snaith, *Nat. Rev. Chem.* **2017**, *1*, 0095.
[37] H. Shen, D. Walter, Y. Wu, K. C. Fong, D. A. Jacobs, T. Duong, J. Peng, K. Weber, T. P. White, K. R. Catchpole, *Adv. Energy Mater.* **2020**, *10*, 1902840.
[38] M. Jošt, L. Kegelmann, L. Korte, S. Albrecht, *Adv. Energy Mater.* **2020**, *10*, 1904102.
[39] M. I. Hossain, W. Qarony, S. Ma, L. Zeng, D. Knipp, Y. H. Tsang, *Nano-Micro Lett.* **2019**, *11*, 58.
[40] H. J. Snaith, S. Lilliu, *Scientific Video Protocols* **2018**, *1*, 1.
[41] B. Chen, N. Ren, Y. Li, L. Yan, S. Mazumdar, Y. Zhao, X. Zhang, *Adv. Energy Mater.* **2022**, *12*, 2003628.
[42] M. A. Green, Y. Hishikawa, E. Dunlop, D. Levi, J. Hohl-Ebinger, M. Yoshita, A. Ho-Baillie, *Prog. Photovoltaics* **2019**, *27*, 3.
[43] A. Al-Ashouri, E. Köhnen, B. Li, A. Magomedov, H. Hempel, P. Caprioglio, J. A. Márquez, A. B. M. Vilches, E. Kasparavicius, J. A. Smith, N. Phung, D. Menzel, M. Grischek, L. Kegelmann, D. Skroblin, C. Gollwitzer, T. Malinauskas, M. Jošt, G. Matič, B. Rech, R. Schlatmann, M. Topič, L. Korte, A. Abate, B. Stannowski, D. Neher, M. Stolterfoht, T. Unold, V. Getautis, S. Albrecht, et al., *Science* **2020**, *370*, 1300, http://doi.org/10.1126/science.abd4016.
[44] NREL Best Research-Cell Efficiencies Chart **2021**, https://www.nrel.gov/pv/cell-efficiency.html.
[45] M. Xiao, F. Huang, W. Huang, Y. Dkhissi, Y. Zhu, J. Etheridge, A. Gray-Weale, U. Bach, Y. B. Cheng, L. Spiccia, *Angew. Chem., Int. Ed.* **2014**, *53*, 9898.
[46] N. J. Jeon, J. H. Noh, Y. C. Kim, W. S. Yang, S. Ryu, S. I. Seok, *Nat. Mater.* **2014**, *13*, 897.
[47] H. J. Snaith, P. Hacke, *Nat. Energy* **2018**, *3*, 459.
[48] C. Messmer, B. S. Goraya, S. Nold, P. S. C. Schulze, V. Sittinger, J. Schön, J. C. Goldschmidt, M. Bivour, S. W. Glunz, M. Hermle, *Prog. Photovoltaics* **2020**, *29*, 744.
[49] J. Burschka, N. Pellet, S.-J. Moon, R. Humphry-Baker, P. Gao, M. K. Nazeeruddin, M. Grätzel, *Nature* **2013**, *499*, 316.
[50] Y. Wu, D. Yan, J. Peng, Y. Wan, S. P. Phang, H. Shen, N. Wu, C. Barugkin, X. Fu, S. Surve, *Energy Environ. Sci.* **2017**, *10*, 2472.
[51] R. L. Hoye, K. A. Bush, F. Oviedo, S. E. Sofia, M. Thway, X. Li, Z. Liu, J. Jean, J. P. Mailoa, A. Osherov, *IEEE J. Photovoltaics* **2018**, *8*, 1023.
[52] J. Werner, A. Walter, E. Rucavado, S.-J. Moon, D. Sacchetto, M. Rienaecker, R. Peibst, R. Brendel, X. Niquille, S. De Wolf, *Appl. Phys. Lett.* **2016**, *109*, 233902.
[53] H. Shen, S. T. Omelchenko, D. A. Jacobs, S. Yalamanchili, Y. Wan, D. Yan, P. Phang, Y. Wu, Y. Yin, C. Samundsett, *Sci. Adv.* **2018**, *4*, eaau9711.
[54] R. Peibst, M. Rienäcker, B. Min, C. Klamt, R. Niepelt, T. F. Wietler, T. Dullweber, E. Sauter, J. Hübner, M. Oestreich, *IEEE J. Photovoltaics* **2018**, *9*, 49.
[55] G. Nogay, F. Sahli, J. Werner, R. Monnard, M. Boccard, M. Despeisse, F. Haug, Q. Jeangros, A. Ingenito, C. Ballif, *ACS Energy Lett.* **2019**, *4*, 844.
[56] J. Haschke, O. Dupré, M. Boccard, C. Ballif, *Sol. Energy Mater. Sol. Cells* **2018**, *187*, 140.

[57] S. De Wolf, A. Descoeudres, Z. C. Holman, C. Ballif, *Green* **2012**, *2*, 7.
[58] M. Taguchi, A. Yano, S. Tohoda, K. Matsuyama, Y. Nakamura, T. Nishiwaki, K. Fujita, E. Maruyama, *IEEE J. Photovoltaics* **2013**, *4*, 96.
[59] Z. C. Holman, A. Descoeudres, S. De Wolf, C. Ballif, *IEEE J. Photovoltaics* **2013**, *3*, 1243.
[60] J. Haschke, J. P. Seif, Y. Riesen, A. Tomasi, J. Cattin, L. Tous, P. Choulat, M. Aleman, E. Cornagliotti, A. Uruena, *Energy Environ. Sci.* **2017**, *10*, 1196.
[61] B. Chen, Z. Yu, K. Liu, X. Zheng, Y. Liu, J. Shi, D. Spronk, P. N. Rudd, Z. Holman, J. Huang, *Joule* **2019**, *3*, 177.
[62] M. Jošt, E. Köhnen, A. B. Morales-Vilches, B. Lipovšek, K. Jäger, B. Macco, A. Al-Ashouri, J. Krč, L. Korte, B. Rech, *Energy Environ. Sci.* **2018**, *11*, 3511.
[63] K. A. Bush, S. Manzoor, K. Frohna, Z. J. Yu, J. A. Raiford, A. F. Palmstrom, H.-P. Wang, R. Prasanna, S. F. Bent, Z. C. Holman, *ACS Energy Lett.* **2018**, *3*, 2173.
[64] L. Mazzarella, Y.-H. Lin, S. Kirner, A. B. Morales-Vilches, L. Korte, S. Albrecht, E. Crossland, B. Stannowski, C. Case, H. J. Snaith, R. Schlatmann, *Adv. Energy Mater.* **2019**, *9*, 1803241.
[65] B. Chen, J. Y. Zhengshan, S. Manzoor, S. Wang, W. Weigand, Z. Yu, G. Yang, Z. Ni, X. Dai, Z. C. Holman, *Joule* **2020**, *4*, 850.
[66] Y. Hou, E. Aydin, M. De Bastiani, C. Xiao, F. H. Isikgor, D.-J. Xue, B. Chen, H. Chen, B. Bahrami, A. H. Chowdhury, *Science* **2020**, *367*, 1135.
[67] J. Xu, C. C. Boyd, J. Y. Zhengshan, A. F. Palmstrom, D. J. Witter, B. W. Larson, R. M. France, J. Werner, S. P. Harvey, E. J. Wolf, *Science* **2020**, *367*, 1097.
[68] D. Kim, H. J. Jung, I. J. Park, B. W. Larson, S. P. Dunfield, C. Xiao, J. Kim, J. Tong, P. Boonmongkolras, S. G. Ji, *Science* **2020**, *368*, 155.
[69] K. Suwa, L. Cojocaru, K. Wienands, C. Hofmann, P. S. Schulze, A. J. Bett, K. Winkler, J. C. Goldschmidt, S. W. Glunz, H. Nishide, *ACS Appl. Mater. Interfaces* **2020**, *12*, 6496.
[70] E. Lamanna, F. Matteocci, E. Calabrò, L. Serenelli, E. Salza, L. Martini, F. Menchini, M. Izzi, A. Agresti, S. Pescetelli, *Joule* **2020**, *4*, 865.
[71] C. Li, Y. Wang, W. C. H. Choy, *Small Methods* **2020**, *4*, 2000093.
[72] M. De Bastiani, A. S. Subbiah, E. Aydin, F. H. Isikgor, T. G. Allen, S. De Wolf, *Mater. Horiz.* **2020**, *7*, 2791.
[73] S. Bedair, M. Lamorte, J. Hauser, *Appl. Phys. Lett.* **1979**, *34*, 38.
[74] P. Colter, B. Hagar, S. Bedair, *Crystals* **2018**, *8*, 445.
[75] F. Sahli, J. Werner, B. A. Kamino, M. Bräuninger, R. Monnard, B. Paviet-Salomon, L. Barraud, L. Ding, J. J. D. Leon, D. Sacchetto, *Nat. Mater.* **2018**, *17*, 820.
[76] J. P. Mailoa, C. D. Bailie, E. C. Johlin, E. T. Hoke, A. J. Akey, W. H. Nguyen, M. D. McGehee, T. Buonassisi, *Appl. Phys. Lett.* **2015**, *106*, 121105.
[77] S. Albrecht, M. Saliba, J. P. C. Baena, F. Lang, L. Kegelmann, M. Mews, L. Steier, A. Abate, J. Rappich, L. Korte, *Energy Environ. Sci.* **2016**, *9*, 81.
[78] J. Werner, C.-H. Weng, A. Walter, L. Fesquet, J. P. Seif, S. De Wolf, B. Niesen, C. Ballif, *J. Phys. Chem. Lett.* **2016**, *7*, 161.
[79] F. Fu, T. Feurer, T. Jäger, E. Avancini, B. Bissig, S. Yoon, S. Buecheler, A. N. Tiwari, *Nat. Commun.* **2015**, *6*, 8932.
[80] K. A. Bush, A. F. Palmstrom, J. Y. Zhengshan, M. Boccard, R. Cheacharoen, J. P. Mailoa, D. P. McMeekin, R. L. Hoye, C. D. Bailie, T. Leijtens, I. M. Peters, M. C. Minichetti, N. Rolston, R. Prasanna, S. Sofia, D. Harwood, W. Ma, F. Moghadam, H. J. Snaith, T. Buonassisi, Z. C. Holman, S. F. Bent, M. D. McGehee, *Nat. Energy* **2017**, *2*, 17009.
[81] K. A. Bush, C. D. Bailie, Y. Chen, A. R. Bowring, W. Wang, W. Ma, T. Leijtens, F. Moghadam, M. D. McGehee, *Adv. Mater.* **2016**, *28*, 3937.
[82] F. Fu, T. Feurer, T. P. Weiss, S. Pisoni, E. Avancini, C. Andres, S. Buecheler, A. N. Tiwari, *Nat. Energy* **2016**, *2*, 16190.
[83] B. A. Kamino, B. Paviet-Salomon, S.-J. Moon, N. Badel, J. Levrat, G. Christmann, A. Walter, A. Faes, L. Ding, J. J. D. Leon, *ACS Appl. Energy Mater.* **2019**, *2*, 3815.
[84] P. S. Schulze, A. J. Bett, M. Bivour, P. Caprioglio, F. M. Gerspacher, Ö. Ş. Kabaklı, A. Richter, M. Stolterfoht, Q. Zhang, D. Neher, *Sol. RRL* **2020**, *4*, 2000152.
[85] E. Köhnen, P. Wagner, F. Lang, A. Cruz, B. Li, M. Roß, M. Jošt, A. B. Morales-Vilches, M. Topič, M. Stolterfoht, D. Neher, L. Korte, B. Rech, R. Schlatmann, B. Stannowski, S. Albrecht, *Sol. RRL* **2021**, *5*, 2100244.
[86] M. Roß, S. Severin, M. B. Stutz, P. Wagner, H. Köbler, M. Favin-Lévêque, A. Al-Ashouri, P. Korb, P. Tockhorn, A. Abate, B. Stannowski, B. Rech, S. Albrecht, *Adv. Energy Mater.* **2021**, *11*, 2101460.
[87] E. Aydin, T. G. Allen, M. De Bastiani, L. Xu, J. Ávila, M. Salvador, E. Van Kerschaver, S. De Wolf, *Nat. Energy* **2020**, *5*, 851.
[88] F. H. Isikgor, F. Furlan, J. Liu, E. Ugur, M. K. Eswaran, A. S. Subbiah, E. Yengel, M. De Bastiani, G. T. Harrison, S. Zhumagali, *Joule* **2021**, *5*, 1566.
[89] J. Werner, L. Barraud, A. Walter, M. Bräuninger, F. Sahli, D. Sacchetto, N. Tétreault, B. Paviet-Salomon, S.-J. Moon, C. Allebé, *ACS Energy Lett.* **2016**, *1*, 474.
[90] S. Essig, C. Allebé, T. Remo, J. F. Geisz, M. A. Steiner, K. Horowitz, L. Barraud, J. S. Ward, M. Schnabel, A. Descoeudres, D. L. Young, M. Woodhouse, M. Despeisse, C. Ballif, A. Tamboli, *Nat. Energy* **2017**, *2*, 17144.
[91] M. A. Green, E. D. Dunlop, J. Hohl-Ebinger, M. Yoshita, N. Kopidakis, X. Hao, *Progress in Photovoltaics: Research Applications* **2020**, *28*, 629.
[92] F. Sahli, B. A. Kamino, J. Werner, M. Bräuninger, B. Paviet-Salomon, L. Barraud, R. Monnard, J. P. Seif, A. Tomasi, Q. Jeangros, *Adv. Energy Mater.* **2018**, *8*, 1701609.
[93] M. Morales-Masis, S. De Wolf, R. Woods-Robinson, J. W. Ager, C. Ballif, *Adv. Electron. Mater.* **2017**, *3*, 1600529.
[94] E. Aydin, M. De Bastiani, X. Yang, M. Sajjad, F. Aljamaan, Y. Smirnov, M. N. Hedhili, W. Liu, T. G. Allen, L. Xu, *Adv. Funct. Mater.* **2019**, *29*, 1901741.
[95] B. Chen, S.-W. Baek, Y. Hou, E. Aydin, M. De Bastiani, B. Scheffel, A. Proppe, Z. Huang, M. Wei, Y.-K. Wang, E.-H. Jung, T. G. Allen, E. V. Kerschaver, F. P. G. de Arquer, M. I. Saidaminov, S. Hoogland, S. De Wolf, E. H. Sargent, *Nat. Commun.* **2020**, *11*, 1257.
[96] S. Altazin, L. Stepanova, J. Werner, B. Niesen, C. Ballif, B. Ruhstaller, *Opt. Express* **2018**, *26*, A579.
[97] D. A. Jacobs, M. Langenhorst, F. Sahli, B. S. Richards, T. P. White, C. Ballif, K. R. Catchpole, U. W. Paetzold, *J. Phys. Chem. Lett.* **2019**, *10*, 3159.
[98] M. Green, E. Dunlop, J. Hohl-Ebinger, M. Yoshita, N. Kopidakis, X. Hao, *Prog. Photovoltaics* **2021**, *29*, 3.
[99] M. Boccard, C. Ballif, *ACS Energy Lett.* **2020**, *5*, 1077.
[100] E. Köhnen, M. Jošt, A. B. Morales-Vilches, P. Tockhorn, A. Al-Ashouri, B. Macco, L. Kegelmann, L. Korte, B. Rech, R. Schlatmann, B. Stannowski, S. Albrecht, *Sustainable Energy Fuels* **2019**, *3*, 1995.
[101] M. T. Hörantner, T. Leijtens, M. E. Ziffer, G. E. Eperon, M. G. Christoforo, M. D. McGehee, H. J. Snaith, *ACS Energy Lett.* **2017**, *2*, 2506.
[102] J. Werner, F. Sahli, F. Fu, J. J. D. Leon, A. Walter, B. A. Kamino, B. Niesen, S. Nicolay, Q. Jeangros, C. Ballif, *ACS Energy Lett.* **2018**, *3*, 2052.
[103] E. T. Hoke, D. J. Slotcavage, E. R. Dohner, A. R. Bowring, H. I. Karunadasa, M. D. McGehee, *Chem. Sci.* **2015**, *6*, 613.
[104] S. Mahesh, J. M. Ball, R. D. Oliver, D. P. McMeekin, P. K. Nayak, M. B. Johnston, H. J. J. E. Snaith, *Energy Environ. Sci.* **2020**, *13*, 258.

[105] E. Unger, L. Kegelmann, K. Suchan, D. Sörell, L. Korte, S. Albrecht, *J. Mater. Chem. A* **2017**, *5*, 11401.
[106] T. C.-J. Yang, P. Fiala, Q. Jeangros, C. Ballif, *Joule* **2018**, *2*, 1421.
[107] M. Stolterfoht, M. Grischek, P. Caprioglio, C. M. Wolff, E. Gutierrez-Partida, F. Peña-Camargo, D. Rothhardt, S. Zhang, M. Raoufi, J. Wolansky, *Adv. Mater.* **2020**, *32*, 2000080.
[108] M. Abdi-Jalebi, Z. Andaji-Garmaroudi, S. Cacovich, C. Stavrakas, B. Philippe, J. M. Richter, M. Alsari, E. P. Booker, E. M. Hutter, A. J. Pearson, *Nat. Energy* **2018**, *555*, 497.
[109] Q. Jiang, Y. Zhao, X. Zhang, X. Yang, Y. Chen, Z. Chu, Q. Ye, X. Li, Z. Yin, J. You, *Nat. Photonics* **2019**, *13*, 460.
[110] A. Al-Ashouri, A. Magomedov, M. Roß, M. Jošt, M. Talaikis, G. Chistiakova, T. Bertram, J. A. Márquez, E. Köhnen, E. Kasparavičius, *Energy Environ. Sci.* **2019**, *12*, 3356.
[111] C. M. Wolff, L. Canil, C. Rehermann, N. N. Linh, F. Zu, M. Ralaiarisoa, P. Caprioglio, L. Fiedler, M. Stolterfoht, S. Kogikoski Jr., *ACS Nano* **2020**, *14*, 1445.
[112] S. Gharibzadeh, B. A. Nejand, M. Jakoby, T. Abzieher, D. Hauschild, S. Moghadamzadeh, J. A. Schwenzer, P. Brenner, R. Schmager, A. A. Haghighirad, *Adv. Energy Mater.* **2019**, *9*, 1803699.
[113] M. A. Mahmud, T. Duong, Y. Yin, H. T. Pham, D. Walter, J. Peng, Y. Wu, L. Li, H. Shen, N. Wu, *Adv. Funct. Mater.* **2020**, *30*, 1907962.
[114] A. F. Palmstrom, G. E. Eperon, T. Leijtens, R. Prasanna, S. N. Habisreutinger, W. Nemeth, E. A. Gaulding, S. P. Dunfield, M. Reese, S. Nanayakkara, *Joule* **2019**, *3*, 2193.
[115] G. E. Eperon, K. H. Stone, L. E. Mundt, T. H. Schloemer, S. N. Habisreutinger, S. P. Dunfield, L. T. Schelhas, J. J. Berry, D. T. Moore, *ACS Energy Lett.* **2020**, *5*, 1856.
[116] T. W. Jones, A. Osherov, M. Alsari, M. Sponseller, B. C. Duck, Y.-K. Jung, C. Settens, F. Niroui, R. Brenes, C. V. Stan, *Energy Environ. Sci.* **2019**, *12*, 596.
[117] E. M. Tennyson, T. A. Doherty, S. D. Stranks, *Nat. Rev. Mater.* **2019**, *4*, 573.
[118] S. De Wolf, J. Holovsky, S.-J. Moon, P. Löper, B. Niesen, M. Ledinsky, F.-J. Haug, J.-H. Yum, C. Ballif, *J. Phys. Chem. Lett.* **2014**, *5*, 1035.
[119] M. Ledinsky, T. Schönfeldová, J. Holovský, E. Aydin, Z. Hájková, L. Landová, N. Neyková, A. Fejfar, S. De Wolf, *J. Phys. Chem. Lett.* **2019**, *10*, 1368.
[120] D. Luo, W. Yang, Z. Wang, A. Sadhanala, Q. Hu, R. Su, R. Shivanna, G. F. Trindade, J. F. Watts, Z. Xu, *Science* **2018**, *360*, 1442.
[121] Z. Liu, L. Krückemeier, B. Krogmeier, B. Klingebiel, J. A. Márquez, S. Levcenko, S. Öz, S. Mathur, U. Rau, T. Unold, *ACS Energy Lett.* **2018**, *4*, 110.
[122] P. K. Nayak, S. Mahesh, H. J. Snaith, D. Cahen, *Nat. Rev. Mat.* **2019**, *4*, 269.
[123] Z. Li, T. R. Klein, D. H. Kim, M. Yang, J. J. Berry, M. F. Van Hest, K. Zhu, *Nat. Rev. Mater.* **2018**, *3*, 18017.
[124] A. Ren, H. Lai, X. Hao, Z. Tang, H. Xu, B. M. F. Y. Jeco, K. Watanabe, L. Wu, J. Zhang, M. Sugiyama, *Joule* **2020**, *4*, 1263.
[125] M. A. Green, E. D. Dunlop, J. Hohl-Ebinger, M. Yoshita, N. Kopidakis, X. Hao, *Prog. Photovoltaics* **2021**, *29*, 657.
[126] J. Zheng, H. Mehrvarz, C. Liao, J. Bing, X. Cui, Y. Li, V. R. Gonçales, C. F. J. Lau, D. S. Lee, Y. Li, *ACS Energy Lett.* **2019**, *4*, 2623.
[127] X. Li, W. Zhang, X. Guo, C. Lu, J. Wei, J. Fang, *Science* **2022**, *375*, 434.
[128] X. Zheng, Y. Hou, C. Bao, J. Yin, F. Yuan, Z. Huang, K. Song, J. Liu, J. Troughton, N. Gasparini, *Nat. Energy* **2020**, *5*, 131.
[129] Y. Yu, F. Zhang, T. Hou, X. Sun, H. Yu, M. Zhang, *Sol. RRL* **2021**, *5*, 2100386.
[130] A. Babayigit, J. D'Haen, H.-G. Boyen, B. Conings, *Joule* **2018**, *2*, 1205.
[131] S. Tang, J. Bing, J. Zheng, J. Tang, Y. Li, M. Mayyas, Y. Cho, T. W. Jones, T. C.-J. Yang, L. Yuan, M. Tebyetekerwa, H. T. Nguyen, M. P. Nielsen, N. J. Ekins-Daukes, K. Kalantar-Zadeh, G. J. Wilson, D. R. McKenzie, S. Huang, A. W. Y. Ho-Baillie, *Cell Rep. Phys. Sci.* **2021**, *2*, 100511.
[132] J. Werner, T. Moot, T. A. Gossett, I. E. Gould, A. F. Palmstrom, E. J. Wolf, C. C. Boyd, M. F. A. M. van Hest, J. M. Luther, J. J. Berry, M. D. McGehee, *ACS Energy Lett.* **2020**, *5*, 1215.
[133] Y. Deng, E. Peng, Y. Shao, Z. Xiao, Q. Dong, J. Huang, *Energy Environ. Sci.* **2015**, *8*, 1544.
[134] S. Tang, Y. Deng, X. Zheng, Y. Bai, Y. Fang, Q. Dong, H. Wei, J. Huang, *Adv. Energy Mater.* **2017**, *7*, 1700302.
[135] Y. Deng, X. Zheng, Y. Bai, Q. Wang, J. Zhao, J. Huang, *Nat. Energy* **2018**, *3*, 560.
[136] W.-Q. Wu, Q. Wang, Y. Fang, Y. Shao, S. Tang, Y. Deng, H. Lu, Y. Liu, T. Li, Z. Yang, A. Gruverman, J. Huang, *Nat. Commun.* **2018**, *9*, 1625.
[137] W.-Q. Wu, Z. Yang, P. N. Rudd, Y. Shao, X. Dai, H. Wei, J. Zhao, Y. Fang, Q. Wang, Y. Liu, *Sci. Adv.* **2019**, *5*, eaav8925.
[138] Y. Deng, C. H. Van Brackle, X. Dai, J. Zhao, B. Chen, J. Huang, *Sci. Adv.* **2019**, *5*, eaax7537.
[139] S. Chen, X. Dai, S. Xu, H. Jiao, L. Zhao, J. Huang, *Science* **2021**, *373*, 902.
[140] Y. Deng, S. Xu, S. Chen, X. Xiao, J. Zhao, J. Huang, *Nat. Energy* **2021**, *6*, 633.
[141] N.-G. Park, K. Zhu, *Nat. Rev. Mater.* **2020**, *5*, 333.
[142] D. H. Kim, J. B. Whitaker, Z. Li, M. F. van Hest, K. Zhu, *Joule* **2018**, *2*, 1437.
[143] M. Xu, W. Ji, Y. Sheng, Y. Wu, H. Cheng, J. Meng, Z. Yan, J. Xu, A. Mei, Y. Hu, *Nano Energy* **2020**, *74*, 104842.
[144] T. Bu, J. Li, H. Li, C. Tian, J. Su, G. Tong, L. K. Ono, C. Wang, Z. Lin, N. Chai, *Science* **2021**, *372*, 1327.
[145] S. Sansoni, M. De Bastiani, E. Aydin, E. Ugur, F. H. Isikgor, A. Al-Zahrani, F. Lamberti, F. Laquai, M. Meneghetti, S. De Wolf, *Adv. Mater. Technol.* **2020**, *5*, 1901009.
[146] X. Peng, J. Yuan, S. Shen, M. Gao, A. S. Chesman, H. Yin, J. Cheng, Q. Zhang, D. Angmo, *Adv. Funct. Mater.* **2017**, *27*, 1703704.
[147] J. Ávila, C. Momblona, P. P. Boix, M. Sessolo, H. J. Bolink, *Joule* **2017**, *1*, 431.
[148] Y. Vaynzof, *Adv. Energy Mater.* **2020**, *10*, 2003073.
[149] Q. Guesnay, F. Sahli, C. Ballif, Q. Jeangros, *APL Mater.* **2021**, *9*, 100703.
[150] M. Liu, M. B. Johnston, H. J. Snaith, *Nature* **2013**, *501*, 395.
[151] C. Momblona, L. Gil-Escrig, E. Bandiello, E. M. Hutter, M. Sessolo, K. Lederer, J. Blochwitz-Nimoth, H. J. Bolink, *Energy Environ. Sci.* **2016**, *9*, 3456.
[152] G. Longo, C. Momblona, M.-G. La-Placa, L. n. Gil-Escrig, M. Sessolo, H. J. Bolink, *ACS Energy Lett.* **2017**, *3*, 214.
[153] L. Gil-Escrig, C. Momblona, M. G. La-Placa, P. P. Boix, M. Sessolo, H. J. Bolink, *Adv. Energy Mater.* **2018**, *8*, 1703506.
[154] J. Li, H. Wang, X. Y. Chin, H. A. Dewi, K. Vergeer, T. W. Goh, J. W. M. Lim, J. H. Lew, K. P. Loh, C. Soci, *Joule* **2020**, *4*, 1035.
[155] L. Cojocaru, K. Wienands, T. W. Kim, S. Uchida, A. J. Bett, S. Rafizadeh, J. C. Goldschmidt, S. W. Glunz, *ACS Appl. Mater. Interfaces* **2018**, *10*, 26293.
[156] T. Abzieher, J. A. Schwenzer, S. Moghadamzadeh, F. Sutterlüti, I. M. Hossain, M. Pfau, E. Lotter, M. Hetterich, B. S. Richards, U. Lemmer, *IEEE J. Photovoltaics* **2019**, *9*, 1249.
[157] K. Hamada, K. Yonezawa, K. Yamamoto, T. Taima, S. Hayase, N. Ooyagi, Y. Yamamoto, K. Ohdaira, *Jpn. J. Appl. Phys.* **2019**, *58*, SBBF06.
[158] J. Li, H. A. Dewi, H. Wang, J. Zhao, N. Tiwari, N. Yantara, T. Malinauskas, V. Getautis, T. J. Savenije, N. Mathews, S. Mhaisalkar, A. Bruno, *Adv. Funct. Mater.* **2021**, *31*, 2103252.

[159] T. Abzieher, T. Feeney, F. Schackmar, Y. J. Donie, I. M. Hossain, J. A. Schwenzer, T. Hellmann, T. Mayer, M. Powalla, U. W. Paetzold, *Adv. Funct. Mater.* **2021**, *31*, 2104482.
[160] D. B. Mitzi, M. Prikas, K. Chondroudis, *Chem. Mater.* **1999**, *11*, 542.
[161] G. Longo, L. Gil-Escrig, M. J. Degen, M. Sessolo, H. J. Bolink, *Chem. Commun.* **2015**, *51*, 7376.
[162] G. Liang, H. Lan, P. Fan, C. Lan, Z. Zheng, H. Peng, J. Luo, *Coatings* **2018**, *8*, 256.
[163] N. K. Noel, S. N. Habisreutinger, B. Wenger, M. T. Klug, M. T. Hörantner, M. B. Johnston, R. J. Nicholas, D. T. Moore, H. J. Snaith, *Energy Environ. Sci.* **2017**, *10*, 145.
[164] F. Fu, L. Kranz, S. Yoon, J. Löckinger, T. Jäger, J. Perrenoud, T. Feurer, C. Gretener, S. Buecheler, A. N. Tiwari, *Phys. Status Solidi* **2015**, *212*, 2708.
[165] C. Tao, S. Neutzner, L. Colella, S. Marras, A. R. S. Kandada, M. Gandini, M. De Bastiani, G. Pace, L. Manna, M. Caironi, *Energy Environ. Sci.* **2015**, *8*, 2365.
[166] F. Fu, S. Pisoni, T. P. Weiss, T. Feurer, A. Wäckerlin, P. Fuchs, S. Nishiwaki, L. Zortea, A. N. Tiwari, S. Buecheler, *Adv. Sci.* **2018**, *5*, 1700675.
[167] L. Qiu, S. He, Y. Jiang, D.-Y. Son, L. K. Ono, Z. Liu, T. Kim, T. Bouloumis, S. Kazaoui, Y. Qi, *J. Mater. Chem. A* **2019**, *7*, 6920.
[168] S. Siegrist, S.-C. Yang, E. Gilshtein, X. Sun, A. N. Tiwari, F. Fu, *J. Mater. Chem. A* **2021**, *9*, 26680.
[169] A. Faes, A. Lachowicz, A. Bettinelli, P.-J. Ribeyron, J. Lerat, D. Munoz, J. Geissbühler, H. Li, C. Ballif, M. Despeisse, *Photovoltaics Int.* **2018**, *41*, 65.
[170] T. Hatt, Ö. Ş. Kabakli, P. S. C. Schulze, A. Richter, S. W. Glunz, M. Glatthaar, J. C. Goldschmidt, J. Bartsch, *Sol. RRL* **2021**, *5*, 2100381.
[171] A. Rehman, E. P. Van Kerschaver, E. Aydin, W. Raja, T. G. Allen, S. De Wolf, *Progress in Photovoltaics: Research and Applications* **2021**, http://doi.org/10.1002/pip.3499.
[172] J. Qian, A. Thomson, Y. Wu, K. Weber, A. Blakers, *ACS Appl. Energy Mater.* **2018**, *1*, 3025.
[173] M. Jaysankar, M. Filipič, B. Zielinski, R. Schmager, W. Song, W. Qiu, U. W. Paetzold, T. Aernouts, M. Debucquoy, R. Gehlhaar, *Energy Environ. Sci.* **2018**, *11*, 1489.
[174] H. J. Snaith, A. Abate, J. M. Ball, G. E. Eperon, T. Leijtens, N. K. Noel, S. D. Stranks, J. T.-W. Wang, K. Wojciechowski, W. Zhang, *J. Phys. Chem. Lett.* **2014**, *5*, 1511.
[175] C. Eames, J. M. Frost, P. R. F. Barnes, B. C. O'Regan, A. Walsh, M. S. Islam, *Nat. Commun.* **2015**, *6*, 7497.
[176] S. Reichert, Q. An, Y.-W. Woo, A. Walsh, Y. Vaynzof, C. Deibel, *Nat. Commun.* **2020**, *11*, 6098.
[177] N. Rolston, B. L. Watson, C. D. Bailie, M. D. McGehee, J. P. Bastos, R. Gehlhaar, J.-E. Kim, D. Vak, A. T. Mallajosyula, G. Gupta, *Extreme Mech. Lett.* **2016**, *9*, 353.
[178] N. Rolston, A. D. Printz, J. M. Tracy, H. C. Weerasinghe, D. Vak, L. J. Haur, A. Priyadarshi, N. Mathews, D. J. Slotcavage, M. D. McGehee, *Adv. Energy Mater.* **2018**, *8*, 1702116.
[179] F. Matteocci, L. Cinà, E. Lamanna, S. Cacovich, G. Divitini, P. A. Midgley, C. Ducati, A. Di Carlo, *Nano Energy* **2016**, *30*, 162.
[180] R. Cheacharoen, C. C. Boyd, G. F. Burkhard, T. Leijtens, J. A. Raiford, K. A. Bush, S. F. Bent, M. D. McGehee, *Sustainable Energy Fuels* **2018**, *2*, 2398.
[181] A. Uddin, M. B. Upama, H. Yi, L. Duan, *Coatings* **2019**, *9*, 65.
[182] C. Case, N. Beaumont, D. Kirk, *ACS Energy Lett.* **2019**, *4*, 2760.
[183] P. Holzhey, M. Saliba, *J. Mater. Chem. A* **2018**, *6*, 21794.
[184] R. Cheacharoen, N. Rolston, D. Harwood, K. A. Bush, R. H. Dauskardt, M. D. McGehee, *Energy Environ. Sci.* **2018**, *11*, 144.
[185] L. Shi, M. P. Bucknall, T. L. Young, M. Zhang, L. Hu, J. Bing, J. Kim, T. Wu, N. Takamure, D. R. McKenzie, S. Huang, M. A. Green, A. W. Y. Ho-Baillie, *Science* **2020**, *368*, eaba2412.
[186] M. V. Khenkin, E. A. Katz, A. Abate, G. Bardizza, J. J. Berry, C. Brabec, F. Brunetti, V. Bulović, Q. Burlingame, A. Di Carlo, *Nat. Energy* **2020**, *5*, 35.
[187] C. C. Boyd, R. Cheacharoen, T. Leijtens, M. D. McGehee, *Chem. Rev.* **2018**, *119*, 3418.
[188] S. He, L. Qiu, L. K. Ono, Y. Qi, *Mater. Sci. Eng., R* **2020**, *140*, 100545.
[189] R. Wang, M. Mujahid, Y. Duan, Z. K. Wang, J. Xue, Y. Yang, *Adv. Funct. Mater.* **2019**, *29*, 1808843.
[190] L. K. Ono, Y. Qi, S. F. Liu, *Joule* **2018**, *2*, 1961.
[191] R. B. Dunbar, B. C. Duck, T. Moriarty, K. F. Anderson, N. W. Duffy, C. J. Fell, J. Kim, A. Ho-Baillie, D. Vak, Y. Wu, *J. Mater. Chem. A* **2017**, *5*, 22542.
[192] M. De Bastiani, E. Van Kerschaver, Q. Jeangros, A. Ur Rehman, E. Aydin, F. H. Isikgor, A. J. Mirabelli, M. Babics, J. Liu, S. Zhumagali, *ACS Energy Lett.* **2021**, *6*, 2944.
[193] M. Saliba, T. Matsui, J.-Y. Seo, K. Domanski, J.-P. Correa-Baena, M. K. Nazeeruddin, S. M. Zakeeruddin, W. Tress, A. Abate, A. Hagfeldt, *Energy Environ. Sci.* **2016**, *9*, 1989.
[194] S. Wang, Y. Jiang, E. J. Juarez-Perez, L. K. Ono, Y. Qi, *Nat. Energy* **2016**, *2*, 16195.
[195] F. Fu, S. Pisoni, Q. Jeangros, J. Sastre-Pellicer, M. Kawecki, A. Paracchino, T. Moser, J. Werner, C. Andres, L. Duchêne, *Energy Environ. Sci.* **2019**, *12*, 3074.
[196] L. Wang, H. Zhou, J. Hu, B. Huang, M. Sun, B. Dong, G. Zheng, Y. Huang, Y. Chen, L. Li, *Science* **2019**, *363*, 265.
[197] Y.-H. Lin, N. Sakai, P. Da, J. Wu, H. C. Sansom, A. J. Ramadan, S. Mahesh, J. Liu, R. D. Oliver, J. Lim, *Science* **2020**, *369*, 96.
[198] S. Yang, S. Chen, E. Mosconi, Y. Fang, X. Xiao, C. Wang, Y. Zhou, Z. Yu, J. Zhao, Y. Gao, *Science* **2019**, *365*, 473.
[199] J. A. Raiford, C. C. Boyd, A. F. Palmstrom, E. J. Wolf, B. A. Fearon, J. J. Berry, M. D. McGehee, S. F. Bent, *Adv. Energy Mater.* **2019**, *9*, 1902353.
[200] R. A. Razera, D. A. Jacobs, F. Fu, P. Fiala, M. Dussouillez, F. Sahli, T. C. Yang, L. Ding, A. Walter, A. F. Feil, *J. Mater. Chem. A* **2020**, *8*, 242.
[201] C. C. Boyd, R. Cheacharoen, K. A. Bush, R. Prasanna, T. Leijtens, M. D. McGehee, *ACS Energy Lett.* **2018**, *3*, 1772.
[202] S. Bai, P. Da, C. Li, Z. Wang, Z. Yuan, F. Fu, M. Kawecki, X. Liu, N. Sakai, J. T.-W. Wang, *Nat. Energy* **2019**, *571*, 245.
[203] K. Domanski, J.-P. Correa-Baena, N. Mine, M. K. Nazeeruddin, A. Abate, M. Saliba, W. Tress, A. Hagfeldt, M. Grätzel, *ACS Nano* **2016**, *10*, 6306.
[204] S. Bai, P. Da, C. Li, Z. Wang, Z. Yuan, F. Fu, M. Kawecki, X. Liu, N. Sakai, J. T.-W. Wang, *Nature* **2019**, *571*, 245.
[205] Y. Yuan, J. Huang, *Acc. Chem. Res.* **2016**, *49*, 286.
[206] C. Eames, J. M. Frost, P. R. Barnes, B. C. O'regan, A. Walsh, M. S. Islam, *Nat. Commun.* **2015**, *6*, 7497.
[207] Z. Xiao, Y. Yuan, Y. Shao, Q. Wang, Q. Dong, C. Bi, P. Sharma, A. Gruverman, J. Huang, *Nat. Mater.* **2015**, *14*, 193.
[208] Q. Jeangros, M. Duchamp, J. Werner, M. Kruth, R. E. Dunin-Borkowski, B. Niesen, C. Ballif, A. Hessler-Wyser, *Nano Lett.* **2016**, *16*, 7013.
[209] M. I. Saidaminov, J. Kim, A. Jain, R. Quintero-Bermudez, H. Tan, G. Long, F. Tan, A. Johnston, Y. Zhao, O. Voznyy, *Nat. Energy* **2018**, *3*, 648.
[210] M. Abdi-Jalebi, Z. Andaji-Garmaroudi, S. Cacovich, C. Stavrakas, B. Philippe, J. M. Richter, M. Alsari, E. P. Booker, E. M. Hutter, A. J. Pearson, *Nature* **2018**, *555*, 497.
[211] Y. Zong, Y. Zhou, Y. Zhang, Z. Li, L. Zhang, M.-G. Ju, M. Chen, S. Pang, X. C. Zeng, N. P. Padture, *Chem* **2018**, *4*, 1404.
[212] S. G. Motti, D. Meggiolaro, A. J. Barker, E. Mosconi, C. A. R. Perini, J. M. Ball, M. Gandini, M. Kim, F. De Angelis, A. Petrozza, *Nat. Photonics* **2019**, *13*, 532.

[213] S. Meloni, T. Moehl, W. Tress, M. Franckevičius, M. Saliba, Y. H. Lee, P. Gao, M. K. Nazeeruddin, S. M. Zakeeruddin, U. Rothlisberger, M. Graetzel, *Nat. Commun.* **2016**, *7*, 10334.
[214] Y. Kato, L. K. Ono, M. V. Lee, S. Wang, S. R. Raga, Y. Qi, *Adv. Mater. Interfaces* **2015**, *2*, 1500195.
[215] S. Cacovich, L. Cinà, F. Matteocci, G. Divitini, P. A. Midgley, A. Di Carlo, C. Ducati, *Nanoscale* **2017**, *9*, 4700.
[216] Y. Jiang, S.-C. Yang, Q. Jeangros, S. Pisoni, T. Moser, S. Buecheler, A. N. Tiwari, F. Fu, *Joule* **2020**, *4*, 1087.
[217] M. Kaltenbrunner, G. Adam, E. D. Głowacki, M. Drack, R. Schwödiauer, L. Leonat, D. H. Apaydin, H. Groiss, M. C. Scharber, M. S. White, *Nat. Mater.* **2015**, *14*, 1032.
[218] S. Deng, Z. Zhang, C. Ju, J. Dong, Z. Xia, X. Yan, T. Xu, G. Xing, *Energy Procedia* **2017**, *130*, 77.
[219] S. Wendlandt, A. Drobisch, T. Buseth, S. Krauter, P. Grunow, in *25th European Photovoltaic Solar Energy Conference and Exhibition/5th World Conference on Photovoltaic Energy Conversio*, Valencia, Spain, 2010, pp. 4002–4006
[220] A. R. Bowring, L. Bertoluzzi, B. C. O'Regan, M. D. McGehee, *Adv. Energy Mater.* **2018**, *8*, 1702365.
[221] L. Bertoluzzi, J. B. Patel, K. A. Bush, C. C. Boyd, R. A. Kerner, B. C. O'Regan, M. D. McGehee, *Adv. Energy Mater.* **2021**, *11*, 2002614.
[222] D. Bogachuk, K. Saddedine, D. Martineau, S. Narbey, A. Verma, P. Gebhardt, J. P. Herterich, N. Glissmann, S. Zouhair, J. Markert, I. E. Gould, M. D. McGehee, U. Würfel, A. Hinsch, L. Wagner, *Solar RRL* **2021**, 2100527, http://doi.org/10.1002/solr.202100527.
[223] T. Leijtens, G. E. Eperon, S. Pathak, A. Abate, M. M. Lee, H. J. Snaith, *Nat. Commun.* **2013**, *4*, 2885.
[224] F. Bella, G. Griffini, J.-P. Correa-Baena, G. Saracco, M. Grätzel, A. Hagfeldt, S. Turri, C. Gerbaldi, *Science* **2016**, *354*, 203.
[225] J. Zheng, H. Mehrvarz, C. Liao, J. Bing, X. Cui, Y. Li, V. R. Gonçales, C. F. J. Lau, D. S. Lee, Y. Li, M. Zhang, J. Kim, Y. Cho, L. G. Caro, S. Tang, C. Chen, S. Huang, A. W. Y. Ho-Baillie, *ACS Energy Lett.* **2019**, *4*, 2623.
[226] V. Naumann, D. Lausch, A. Hähnel, J. Bauer, O. Breitenstein, A. Graff, M. Werner, S. Swatek, S. Großer, J. Bagdahn, *Sol. Energy Mater. Sol. Cells* **2014**, *120*, 383.
[227] S. P. Harvey, J. Moseley, A. Norman, A. Stokes, B. Gorman, P. Hacke, S. Johnston, M. Al-Jassim, *Prog. Photovoltaics* **2018**, *26*, 377.
[228] S. Yamaguchi, C. Yamamoto, K. Ohdaira, A. Masuda, *Prog. Photovoltaics* **2018**, *26*, 697.
[229] W. Luo, Y. S. Khoo, P. Hacke, V. Naumann, D. Lausch, S. P. Harvey, J. P. Singh, J. Chai, Y. Wang, A. G. Aberle, S. Ramakrishna, *Energy Environ. Sci.* **2017**, *10*, 43.
[230] V. Naumann, K. Ilse, M. Pander, J. Tröndle, K. Sporleder, C. Hagendorf, *AIP Conf. Proc.* **2019**, *2147*, 090005.
[231] U. Varshney, B. Hallam, P. Hamer, A. Ciesla, D. Chen, S. Liu, C. Sen, A. Samadi, M. Abbott, C. Chan, *IEEE J. Photovoltaics* **2019**, *10*, 19.
[232] K. Ramspeck, S. Zimmermann, H. Nagel, A. Metz, Y. Gassenbauer, B. Birkmann, A. Seidl, *Intergovernmental Panel on Climate Change*, Cambridge University Press, Cambridge **2012**, pp. 861–865.
[233] M. De Bastiani, E. Van Kerschaver, Q. Jeangros, A. Ur Rehman, E. Aydin, F. H. Isikgor, A. J. Mirabelli, M. Babics, J. Liu, S. Zhumagali, E. Ugur, G. T. Harrison, T. G. Allen, B. Chen, Y. Hou, S. Shikin, E. H. Sargent, C. Ballif, M. Salvador, S. De Wolf, *Solar RRL.* **2021**, 2100493, http://doi.org/10.1002/solr.202100493.
[234] M. De Bastiani, E. Van Kerschaver, Q. Jeangros, A. Ur Rehman, E. Aydin, F. H. Isikgor, A. J. Mirabelli, M. Babics, J. Liu, S. Zhumagali, E. Ugur, G. T. Harrison, T. G. Allen, B. Chen, Y. Hou, S. Shikin, E. H. Sargent, C. Ballif, M. Salvador, S. De Wolf, *ACS Energy Lett.* **2021**, *6*, 2944.
[235] R. Guerrero-Lemus, R. Vega, T. Kim, A. Kimm, L. Shephard, *Renewable Sustainable Energy Rev.* **2016**, *60*, 1533.
[236] M. De Bastiani, A. J. Mirabelli, Y. Hou, F. Gota, E. Aydin, T. G. Allen, J. Troughton, A. S. Subbiah, F. H. Isikgor, J. Liu, *Nat. Energy* **2021**, *6*, 167.
[237] T. S. Liang, M. Pravettoni, C. Deline, J. S. Stein, R. Kopecek, J. P. Singh, W. Luo, Y. Wang, A. G. Aberle, Y. S. Khoo, *Energy Environ. Sci.* **2019**, *12*, 116.
[238] R. Asadpour, R. V. Chavali, M. R. Khan, M. A. Alam, *Appl. Phys. Lett.* **2015**, *106*, 243902.
[239] H. Chung, X. Sun, A. D. Mohite, R. Singh, L. Kumar, M. A. Alam, P. Bermel, *Opt. Express* **2017**, *25*, A311.
[240] A. H. Onno, Z. C. 45th IEEE PVSC, 28th PVSEC, 34th EUPVSEC, **2018**, pp. 229–232.
[241] L. J. Geerligs, D. Zhang, G. J. M. Janssen, S. L. Luxembourg, *35th European Photovoltaic Solar Energy Conference and Exhibition*, **2018**, pp. 676–680, https://doi.org/10.4229/35thEUPVSEC20182018-2AV.3.23.
[242] J. Lehr, M. Langenhorst, R. Schmager, F. Gota, S. Kirner, U. Lemmer, B. S. Richards, C. Case, U. W. Paetzold, *Sol. Energy Mater. Sol. Cells* **2020**, *208*, 110367.
[243] A. Onno, N. Rodkey, A. Asgharzadeh, S. Manzoor, J. Y. Zhengshan, F. Toor, Z. C. Holman, *Joule* **2020**, *4*, 580.
[244] O. Dupré, A. Tuomiranta, Q. Jeangros, M. Boccard, P.-J. Alet, C. Ballif, *IEEE J. Photovoltaics* **2020**, *10*, 714.
[245] P. Tockhorn, P. Wagner, L. Kegelmann, J.-C. Stang, S. Albrecht, L. Korte, *ACS Appl. Energy Mater.* **2020**, *3*, 1381.
[246] I. J. Park, J. H. Park, S. G. Ji, M.-A. Park, J. H. Jang, J. Y. Kim, *Joule* **2019**, *3*, 807.
[247] E. L. Warren, W. E. McMahon, M. Rienacker, K. T. VanSant, R. C. Whitehead, R. Peibst, A. C. Tamboli, *ACS Energy Lett.* **2020**, *5*, 1233.
[248] W. McMahon, H. Schulte-Huxel, J. Buencuerpo, M. Young, T. Klein, J. Geisz, A. Tamboli, E. Warren Voltage-matched strings using 3-terminal tandems: Fundamentals and end losses. 47th IEEE Photovoltaic Specialists Conference (PVSC), **2020**, 266.
[249] Y. Jiang, L. Qiu, E. J. Juarez-Perez, L. K. Ono, Z. Hu, Z. Liu, Z. Wu, L. Meng, Q. Wang, Y. Qi, *Nat. Energy* **2019**, *4*, 585.
[250] X. Li, F. Zhang, J. Wang, J. Tong, T. Xu, K. Zhu, *Nat. Sustain.* **2021**, *4*, 1038.
[251] S. Chen, Y. Deng, H. Gu, S. Xu, S. Wang, Z. Yu, V. Blum, J. Huang, *Nat. Energy* **2020**, *5*, 1003.
[252] S. Chen, Y. Deng, X. Xiao, S. Xu, P. N. Rudd, J. Huang, *Nat. Sustain.* **2021**, *4*, 636.
[253] B. Chen, C. Fei, S. Chen, H. Gu, X. Xiao, J. Huang, *Nat. Commun.* **2021**, *12*, 5859.
[254] S. Y. Park, J.-S. Park, B. J. Kim, H. Lee, A. Walsh, K. Zhu, D. H. Kim, H. S. Jung, *Nat. Sustain.* **2020**, *3*, 1044.

Fan Fu received his Ph.D. degree from the Swiss Federal Institute of Technology in Zürich (ETH Zürich) in 2017. Subsequently, he joined Prof. Christophe Ballif's group at EPFL as a Postdoctoral Scientist working on textured perovskite-silicon tandem solar cells. Since June 2019, he is group leader in the Laboratory for Thin Films and Photovoltaics at Empa-Swiss Federal Laboratories for Materials Science and Technology. His research focuses on thin film multi-junction photovoltaics. In particular, present research efforts focus on developing efficient and stable perovskite solar cells and mini-modules using industrial relevant scalable methods for tandem applications.

Yi Hou is an Assistant Professor in the Department of Chemical and Biomolecular Engineering at the National University of Singapore (NUS) and the Head of Perovskite-based Multijunction Solar Cell Group at Solar Energy Research Institute of Singapore (SERIS). His Ph.D. is in Materials Science and Engineering at University of Erlangen-Nuremberg in Germany. He is currently leading a research team investigating the photophysical properties of perovskites and their solar cell devices to advance sustainable energy. His group recent efforts focus on the materials innovation, stabilizing the wide-bandgap perovskite absorber layer in photovoltaics, and the upscaling of high-performance perovskite-based tandem solar cells.